

Models for Propagating Facilitation in the Insect Visual System

Pradeep Singh

Computational Science Research Center

San Diego State University

San Diego, California

Spring 2020

Approval Page

Title: Models for Propagating Facilitation in the Insect Visual System

Author: Pradeep Singh

Date Submitted:

Dr. Jose Castillo

Committee Chair

Signature

Dr. Patrick Shoemaker

Advisor & Committee Member

Signature

Dr. Joseph M. Mahaffy

Committee Member

Signature

Copyright © 2020
by
Pradeep Singh

All Rights Reserved

ACKNOWLEDGEMENTS

First and foremost, I wish to express my sincere gratitude and appreciation to my supervisor, Professor Patrick Shoemaker for the continuous support and guidance in my MS study and research. He convincingly guided and encouraged me to be professional and do the right thing even when the road got tough. Without his persistent help, the goal of this project would not have been realized. I could not have imagined having a better advisor and mentor for my MS study.

Besides my advisor, I would like to thank Professor Jose E. Castillo and all other staff members at Computational Science Research Center, SDSU for providing lab space and other infrastructure support for the duration of this project. I also express my thanks to my lab mates; Johnny Corbino and Angel Boada for helping me in my initial days, proofreading my thesis and giving insightful comments.

I wish to acknowledge the support and great love of my family (and friends), my mother, Malkeet Kaur; my Father, Baljinder Singh and three of my close friends, Sushil Raut, Neha Patil and Akash Revankar. They kept me going on and this work would not have been possible without their support.

Finally, I would also like to thanks sponsors of this project. This MS Research was supported by the Air Force Office of Scientific Research, USAF, under grant number FA9550-16-1-0153.

TABLE OF CONTENTS:

1. Abstract
2. List of Tables
3. List of Figures
4. Introduction
5. Response Facilitation
 - 5.1. Response Facilitation
 - 5.2. Experiments for Facilitation
 - 5.3. Nature of Facilitation
 - 5.4. Transmission of Facilitation
6. Anatomy and Physiology of STMD systems
7. Problem Statement
8. Mechanism for Facilitations
 - 8.1. Network of cells
 - 8.2. Regenerative mechanism
 - 8.3. Propagation speed
9. Background
 - 9.1. Glia Cells
 - 9.2. Neurons
 - 9.3. Ca Signaling & Waves
 - 9.3.1. Triggering calcium waves in Astrocytes
 - 9.3.2. Propagation of calcium waves in Astrocytes
 - 9.3.3. Transmission of calcium waves in Astrocytes
 - 9.3.4. Triggering calcium waves in Neurons
 - 9.3.5. Propagation of calcium waves in Neurons
 - 9.3.6. Transmission of calcium waves in Neurons
 - 9.4. Transmission of Ca waves
10. Morphological Structure of Cells
11. Models & Methods
 - 11.1. Propagation of Calcium waves
 - 11.2. Calcium dynamics in Astrocytes
 - 11.2.1. Calcium transport model in Astrocytes
 - 11.2.2. InP3 Receptor kinetics
 - 11.2.3. PIP2 – InP3 – DAG – AA Signaling Cascade
 - 11.2.4. Calcium Pumps in Astrocytes
 - 11.2.5. Calcium buffering in Astrocytes
 - 11.2.6. Gap Junctions in Astrocytes
 - 11.2.7. Leakage Mechanism in Astrocytes
 - 11.2.8. ARC Channels in Astrocytes
 - 11.2.9. Parameters and Constants associated with Astrocyte Model
 - 11.3. Calcium dynamics in Neurons
 - 11.3.1. Calcium transport model in Neurons
 - 11.3.2. Ryanodine receptors in Neurons
 - 11.3.3. Calcium Pumps in Neurons

- 11.3.4. Calcium buffering in Neurons
- 11.3.5. Gap Junctions in Neurons
- 11.3.6. Leakage Mechanism in Neurons
- 11.3.7. Parameters and Constants associated with Neuron Model
- 12. Numerical Simulations
 - 12.1. Mathematical Formulation
 - 12.2. Numerical Solution
 - 12.3. Boundary Conditions
 - 12.4. MOLE Library
- 13. Experiments
 - 13.1. Design of Experiments
 - 13.2. Important Parameters
 - 13.3. Characteristic Examined
 - 13.3.1. Wave Regimes
 - 13.3.1.1. Regenerative Regime
 - 13.3.1.2. Damping Regime
 - 13.3.1.3. Abortive Regime
 - 13.3.2. Wave speed
 - 13.3.3. Wave Amplitude
 - 13.3.4. Region of Influence
 - 13.4. Initiation of Waves
- 14. Results
 - 14.1. Qualitative Results
 - 14.2. Quantitative Results
 - 14.3. Calcium Waves behavior in Networks of Astrocytes
 - 14.3.1. Wavefront in a Network
 - 14.3.2. Theoretical Computation of Wavefront Speed
 - 14.3.3. Observed Wavefront Speed
- 15. Conclusion
- 16. Future Research
- 17. References
- 18. Appendix

1. ABSTRACT

Detecting and tracking moving targets within a visual scene is a complex task. Over thousands of years, many species of animals like flying insects have evolved neural mechanisms for tracking path or location of flying targets that move against the visually cluttered background. Small target motion-detecting (STMD) neurons found in the visual pathway of flying insects display remarkable *selectivity* and *sensitivity* to small moving targets and are thought to support these mechanisms. Contributing to their sensitivity is a form of *facilitation*, in which the responsiveness of an STMD is enhanced by prior exposure to a small target moving along a continuous path in visual space. The locus of facilitation in the receptive field is found to be local to the area of the target and to continue propagating in the direction of target motion even after a stimulus ceases.

In this thesis, we are modeling this phenomenon with the propagation of traveling waves in densely interconnected, retinotopic layers of cells. We hypothesize that waves are initiated and reinforced by the presence of a moving target stimulus, and the network, in turn, interacts with STMDs to modulate their excitability. Membrane potentials travel too fast to play this role, so we have studied and modeled propagating *calcium waves* as a possible mechanism. Accordingly, we have proposed two models that could be the biological substrate for this mechanism: 1) a network of astrocyte-like glia cells, and 2) a network of neurons; both in which calcium waves are initiated by target stimuli and propagate via diffusion with the participation of regenerative mechanisms. Finally we show qualitatively and quantitatively how facilitation would look in any such network and discuss ranges of parameters that would support the facilitation mechanism.

2. LIST OF TABLES

Table 1: List of Astrocytes Model parameter and their baseline values, along with units.....	24
Table 2: List of Neuron Model parameters and their baseline values.	29
Table 3: Model parameters and rate constants that are varied in experiments. For more information on these parameter values and their baseline values, ref Table 1 and 2.	38
Table 4: Parameters related to stimulus. Changing these parameters we can change the strength or region of influence of stimulus on our network.....	40
Table 5: Chart for model parameters and its effects on the Ca wave dynamics. Strong Positive means that increasing parameter value strongly impacts the behavior of waves in positive manner. Strong Negative means that increasing parameter value strongly impacts the behavior of waves in negative manner. NO EFFECT means that change in parameter value have no effect on wave behavior. Small positive and Small negative means that increase in parameter value will have small (less-strong) impact in positive and negative manner. Local and Global means whether the change in parameter value locally will impact locally or globally.	40
Table 6: Table for range of parameter values for different wave behavior. Every parameter is varied separately while keeping other parameters at their baseline value. All experiments were performed on a test bed of two cells with two dendrites each, connected end-to-end.	41
Table 7 Table for Wave velocity (V) with change in parameter value. All experiments are done on a 100 compartment-long single dendrite, where every parameter was varied individually while others were kept constant at their baseline values. Values in red color in every column indicate the baseline value for that parameter. “-“ represents no wave for that set of parameter values. Units for V is uM/s ¹	42
Table 8: Table for Wave amplitude (A) with change in parameter value . All experiments are done on a 100 compartment-long single dendrite, where every parameter was varied once (while others were kept constant at their baseline value). Values in red color in every column are the baseline value for that parameter. “-“ represents no wave for those set of parameter value. Units for V is uM/s.	43
Table 9: Table for Wave speed (V) with change in parameter value . All experiments are done on a single dendrite, where every parameter was varied once (while others were kept constant at their baseline value). Values in red color in every column are the baseline value for that parameter. “-“ represents no wave for those set of parameter value. Units for V is uM/s ¹	43
Table 10: Table for Wave amplitude (A) with change in parameter value . All experiments are done on a single dendrite, where every parameter was varied once (while others were kept constant at their baseline value). Values in red color in every column are the baseline value for that parameter. “-“ represents no wave for those set of parameter value. Units for A is uM.	44

3. LIST OF FIGURES:

- Figure 1: Picture of Electrophysiology Station for conducting Facilitation experiments in dragonflies. The insect (dragonfly) is mounted at center and the display screen is at front left. Image courtesy: David O'Carroll (Lund University).**Error! Bookmark not defined.**15
- Figure 2: A predictive focus facilitates responses to a moving target. Map of facilitation for a priming stimulus consisting of a small target drifted upward partway through the receptive field of identified neuron CSTMD1. The graphics depict a projection onto the upper front quarter of the visual field. The path of the primer is indicated by a vertical black arrow at lower center. Degree of facilitation (change in spike rate in response to probe) is color coded, with warm colors indicating enhanced responsiveness, and cool colors depressed. Panel a depicts the baseline receptive field sensitivity of the neuron, and b depicts the change in sensitivity induced by the primer, when the probe stimuli immediate follow it. In c and d, there is a pause between the end of primer motion and the imposition of the probe stimuli. Image courtesy: David O'Carroll (Lund University) and Steven Wiederman (University of Adelaide).15
- Figure 3: Horizontal section of the optic ganglia of the dragonfly *Hemicordulia tau*. This image is for the right eye, and depicts the first optic ganglion (the lamina), the second (the medulla), and the third (the lobula complex, at left). The primary lobula, shown in pink, is where small-field STMDs receive their inputs, whereas wide-field STMDs arborize elsewhere, including in the medial lobula, the smaller tan structure below the left part of the primary lobula. Image courtesy of J. Fabian, B. el Jundi, S. Wiederman, and D. O'Carroll.16
- Figure 4: Trans-membrane calcium transport model for astrocytes. The buffering action of Calbindin (CalB) is also included for completeness, since like membrane transport it is modeled locally in space. \rightleftharpoons (in black color) represents reversible reactions and \rightleftharpoons (in red color) represents flow of calcium in and out of Ca^{2+} stores. Dotted lines and arrows represents influence of a given molecule/chemical on a reaction; and a + sign represents a positive influence on that reaction. InP3R indicates the InP3 receptor, and R, O, A and I_2 are different states for this receptor's calcium channels; ARC represent Arachidonate-regulated calcium channels. Figure courtesy of Patrick Shoemaker.22
- Figure 5: The Sneyd-Dufour model for InP3 receptor kinetics. Opening of the receptor's calcium channel is associated with states O and A. The functions denoted by ϕ are calcium-dependent rate functions. Transition from the native state R to O involves binding of the ligand InP3, reflected by its presence as a factor in the rate for that transition. The states rendered in gray, I_1 and S, were found to have little participation in receptor function under the conditions we simulated, and are not included in our models. This kinetic structure is associated with each of four subunits of the complete receptor.23

Figure 6: Trans-membrane calcium transport model for neurons. Buffering of calcium by Calbindin is again included for completeness. \rightleftharpoons (in black color) represents reversible reactions and \rightleftharpoons (in red color) represents flow of calcium in and out of cell (and ER) by external input and pumps (SERCA and plasma membrane pumps) respectively, + sign represents positive influence on the reaction, dotted arrow represents influence of a given molecule/chemical on the reaction. C ₂ , O ₁ , C ₁ and O ₂ are different states for RyR receptor's calcium channels. Figure courtesy of Patrick Shoemaker.	30
Figure 7: Single cell in our model.....	33
Figure 8: Two interconnected cell in our model.....	34
Figure 9: Network of 16 astrocytes interconnected together.....	35
Figure 10: 1D staggered grid with Ca source and sink acting on every grid point.....	36
Figure 11: Plane wave approximation. θ is the angle between direction of wave front and perpendicular to plane wave. Dendrites are uniformly distributed with respect to θ and can be anywhere from -90° to 90°.....	46

4. INTRODUCTION

Detecting and tracking moving targets within a visual scene is a complex task, yet it is of great importance to animals that rely on catching or chasing their targets for food and mating. Over thousands of years many species of animal have evolved neural mechanisms for target analysis. Flying insect species like dragonflies show amazing ability to track the path or location of flying targets that move against the visually cluttered background again and again. It has also been stated that dragonflies capture prey with success rate of 97% even in the presences of distractions [1].

Small target motion detector neurons (also known as STMDs) are likely to be involved in this behavior as they display an impressive selectivity for small moving objects [2]. As of now, two relatively higher-order functions have been identified that appear to support this behavior: One is *selective attention* that allows STMDs to respond to a single target at a time [3]; and second is a type of *facilitation* that enhances the response of an STMD to a continuously-moving target [6][27]. Our project focuses on a *facilitation* mechanism that is described as increases in the excitability of a neuron to a continuously-moving target. A number of experiments have been conducted to characterize the process of facilitation and it has been observed that facilitation is predictive in nature [12].

In this project we investigate the predictive aspect of response facilitation by assuming that it might be supported by the propagation of *calcium waves* in a network of astrocyte-like cells or neurons. We model networks of such cells, and then further analysis is done on propagation of calcium signals in this model in presence and absence of external stimulus that corresponds to moving target in real world. We also do comprehensive parametric study of our model, outlining how and why it behaves with different values of parameters and thus characterizing the facilitation mechanism.

5. RESPONSE FACILITATION IN STMDs:

5.1. Response Facilitation:

Facilitation is an increase in excitability of an STMD neuron, dependent upon ongoing excitation by a small-target stimulus. It is not strictly a function of how long an STMD neuron is excited by small targets; rather, its effect is most pronounced when a target moves along a *continuous path* in the visual field [51]. This is a constraint that must be obeyed by the images of real, physical targets – except for periods when they may be occluded by intervening objects. Therefore, we can think of *facilitation* as a means to exploit a natural constraint in order to gain confidence in the target detection mechanism in the actual presence of a target. For the noisy and low-amplitude visual signals that are evoked by small targets, this may give a significant boost to the reliability of detection.

5.2. Experiments for Response Facilitation:

A variety of experiments have been conducted to characterize the process of facilitation. These experiments have been conducted with immobilized insects viewing a screen on which moving small-target stimuli are presented. By analyzing experiments involving intracellular recordings

from individual STMD neurons and examining the sensitivity of the STMDs to small target contrast, Wiederman and O'Carroll and their labs have shown that facilitation corresponds to a modulation of contrast gain in the neural pathway leading to the STMDs.

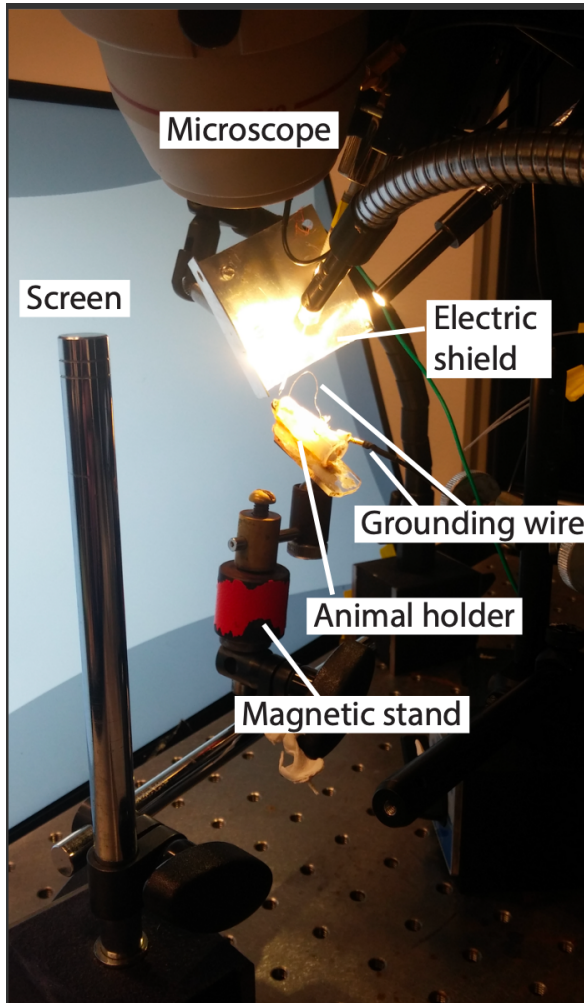


Figure 1: Picture of electrophysiology station for conducting experiments in insects (Bee in this case). The insect is mounted at center on animal holder plate and the display screen is at front left. Image courtesy: Bo Bekkouche (Lund University).

In a critical subset of these experiments [Figure 2], the insects have been subjected to a priming target that moves part way through the receptive field of the STMD and then vanishes, followed by a probe stimulus consisting of a target moving briefly along a short path at some other location. By repeating this sequence for various probe locations, and recording the neural responses, a spatial map of the responsiveness of the STMD following the priming stimulus can be assembled. When this is compared to responsiveness map built without a primer, the degree of facilitation of the neuron due to the primer can be assessed as a function of position in the visual field.

5.3. Nature of Facilitation:

Comparing maps of the receptive field in facilitated and unfacilitated states [Figure 2], it can be seen that the region of facilitation is limited in size and appears at and in front of the last position of the priming stimulus [Ref panel b in Figure 2]. Moreover, when there is a delay between the primer and the probe stimuli, it can be seen that the region of facilitation has actually propagated through space in the direction in which the target was moving [Ref panel c in Figure 2]. These results [Figure 2] clearly show that facilitation can be regarded as spatially local and predictive in nature. Facilitation that doesn't propagate on its own could still translate as a result of the fact that it is evoked by a moving stimulus, but in that case, the facilitation would not keep moving after the stimulus ceases.

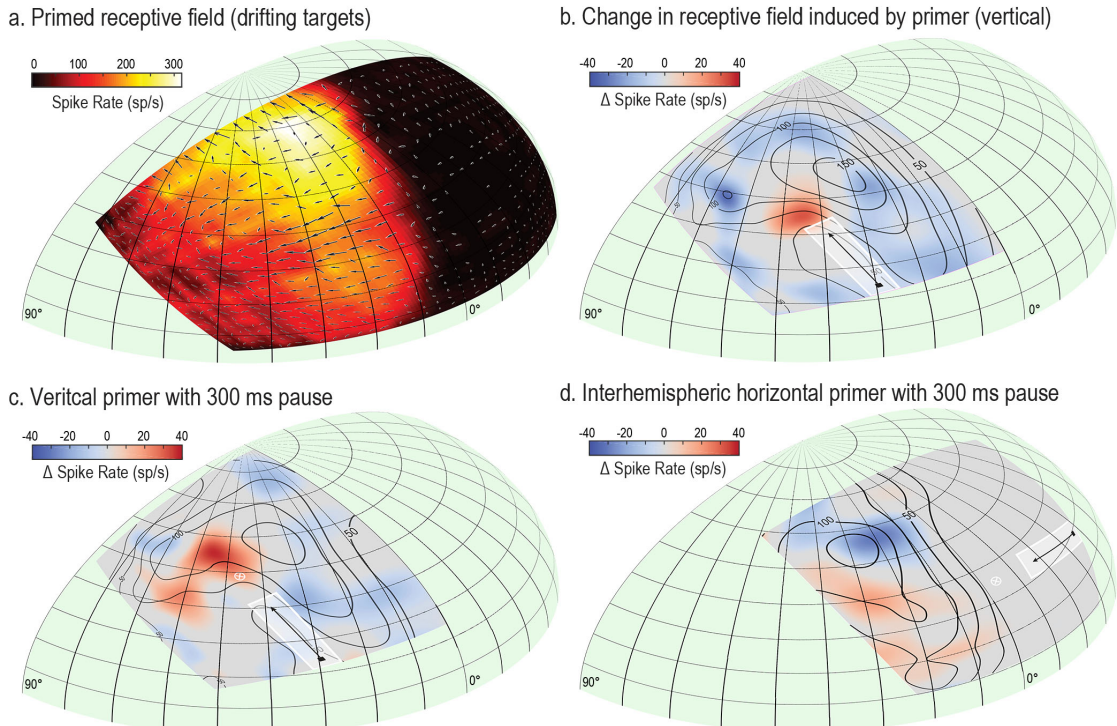


Figure 2: A predictive focus facilitates responses to a moving target. Map of facilitation for a priming stimulus consisting of a small target drifted upward partway through the receptive field of identified neuron CSTMD1. The graphics depict a projection onto the upper front quarter of the visual field. The path of the primer is indicated by a vertical black arrow at lower center. Panel a depicts the excitatory receptive field of this neuron with a color-coding of responses as a function of small target location. Degree of facilitation (change in spike rate in response to probe) is also color coded in panels b-d, with warm colors indicating enhanced responsiveness, and cool colors depressed. Panel b depicts the change in sensitivity induced by the primer, when the probe stimuli immediately follows it. In c and d, there is a pause between the end of primer motion and the imposition of the probe stimuli. Image courtesy: David O'Carroll (Lund University) and Steven Wiederman (University of Adelaide).

5.4. Inter-hemispherical transfer of facilitation:

If we look at panel a of Figure 2, we can see this (monocular) neuron, which only gets direct input from one eye, has excitatory responses only in right hemisphere of brain, whereas a stimulus moving in the left hemisphere is able to induce facilitation in the cell. This suggest that there is transmission of facilitation all the way across the brain. There are likely to be dedicated neurons

that cross over from each side of the brain to the other in order to stimulate facilitation on the opposite side.

6. ANATOMY AND PHYSIOLOGY OF STMD SYSTEMS

The STMDs can be subdivided into many subtypes depending on excitability, direction sensitivity and the size of the receptive field [28]. Two major types defined by their receptive field extents are: wide-field STMDs and small-field STMDs. Small-field STMDs are on the order of 10 degrees in extent and usually oval in shape, while wide-field STMDs, are multiple times larger in area, and in some cases can cover nearly half a visual hemisphere. All STMD cells reside in the third optic ganglion, the lobula, shown at left in Figure 3. There is evidence suggesting that the small-field STMDs, which are located more peripherally than the wide-field STMDs, project their outputs to the wide-field cells. It is not entirely certain at present where the facilitation phenomenon takes place: there is evidence that small-field STMDs, which arborize in the primary lobula and are organized retinotopically, may be subject to facilitation [12] and the locus of the facilitatory ‘hot spot’ is (perhaps not coincidentally) roughly the same size as the receptive fields of small-field STMDs. However, it cannot be ruled out that the moving facilitation takes place where dendritic arborizations of wide-field STMDs occur, such as the medial lobula and other areas deeper in the ganglion. For example, it is plausible that a facilitatory network(s) residing in these regions is stimulated by the small-field inputs that converge on the wide-field STMDs, but then exerts its action on the dendrites of the wide-field neurons themselves.

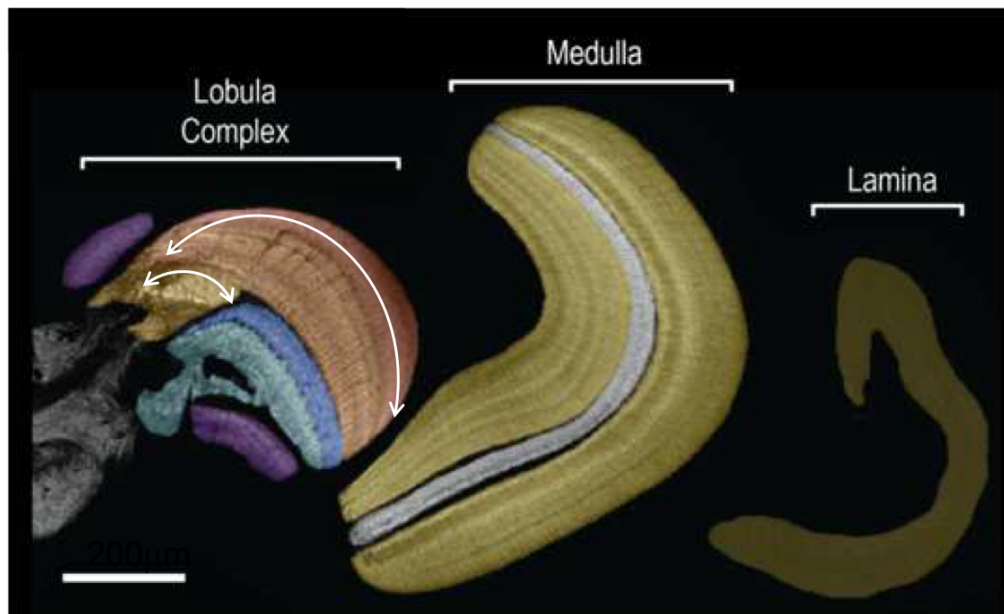


*Figure 3: EMBARGOED Horizontal section of the optic ganglia of the dragonfly *Hemicordulia tau*. This image is for the right eye, and depicts the first optic ganglion (the lamina), the second (the medulla), and the third (the lobula complex, at left). The primary lobula, shown in pink, is where small-field STMDs receive their inputs, whereas wide-field STMDs arborize elsewhere, including in the medial lobula, the smaller tan structure below the left part of the primary lobula. Image courtesy of J. Fabian, B. el Jundi, S. Wiederman, and D. O'Carroll. Release of this figure is embargoed pending publication by its authors.*

It is observed that the region of facilitation moves at a rate of 30-40 degrees/sec in the visual field [12] (with little apparent dependence on stimulus speed [reference personal communication with O'Carroll lab]), which in turn dictates the range of speeds that must be assumed by a propagating signal that mediates the facilitatory process in retinotopic areas of the brain. The outer layers of the primary lobula as seen in Figure 3 span about 750 μm in this horizontal section, corresponding to roughly 135° subtense in visual space; this implies that a moving facilitatory signal in this neuropil would have to propagate at \sim 170 $\mu\text{m}/\text{s}$ to 220 $\mu\text{m}/\text{s}$. Conversely, the medial lobula (also shown in Figure 3), where some wide-field STMDs arborize, is around 1/4 to 1/5 of this size. It is not entirely certain how this structure, or the dendrites of wide-field STMDs in general, scale relative to the visual space they service, but it is clear that required propagation speeds would be smaller, on the order of tens of $\mu\text{m}/\text{s}$, if propagating facilitation takes place there.

7. PROBLEM STATEMENT

Because studies [12] have shown that locus of facilitation induced by a moving target propagates in visual space even after a small target stimulus ceases, we are proposing that it could be supported by traveling wave phenomena in retinotopically-organized regions of the visual system.

We hypothesize that there are some auxiliary layers or two dimensional networks of cells that interact with STMDs; these are stimulated in some way by the moving target stimuli that excite STMDs, possibly through the STMDs themselves. The cellular reaction to this stimulus propagates through the facilitatory network, which can account for propagation of facilitation in space, and the network interacts reciprocally with STMDs, increasing their excitability. This traveling wave (or propagating facilitation) is *reinforced* across the network as a result of a traveling stimulus.

As discussed above, there is a specific speed (range) with which facilitation must propagate in the structures in which such a network could reside; therefore we can say speed is an important constraint. Electrical signals in neurons are a logical possibility to represent facilitation, but these propagate at speeds that are far too great. So, our motivation is to choose models that allow slower wave propagation, and we have identified calcium waves as a plausible candidate. In this thesis, we consider calcium waves in two media: a) an interconnected network of astrocytes, and b) an interconnected network of neurons. These are modeled based on current understanding of the biological processes that support calcium wave propagation, relying on previously-published modeling efforts for this phenomenon.

8. MECHANISM FOR FACILITATION

In this section, we consider the likely features of a biologically-plausible mechanism for predictive facilitation.

8.1. Network of Cells:

Facilitation as a mechanism is spatially local, but it may possibly be universal in the wide-field STMDs and could take place anywhere within the receptive field of many neurons. Therefore, many neurons might be involved in the computation of facilitation over a broad region. Thus, we assume that it is supported by a network of cells that forms a heavily-interconnected, two-dimensional layer or web with many randomly-oriented processes and interconnections between these cells, through which a facilitatory signal can propagate in a roughly isotropic fashion. This

facilitatory signal would be evoked by the same stimuli that elicit activity in STMD neurons, and in turn would affect the excitability of STMD neurons or neural processes with which it interacts.

8.2. Regenerative Mechanism:

The active wave propagation, whether chemical or electrical, requires a regenerative mechanism in order to take place. This regenerative mechanism would involve some form of positive feedback. In any such mechanism, propagating signal causes changes in the cell membrane, like opening of ion channels that further reinforces the signal by influx of more ions that increases signal strength.

8.3. Propagation speed:

A signal that propagates in such a network needs to have a propagation speed less than 1 mm/s, as discussed above. Membrane potentials in cable-like cellular structures are far too fast for our purpose as they have propagation speed on the order of cm/s or more.

8.4. Calcium waves as a mechanism for facilitation

Calcium signaling in recent decades has gained lot of attention, and recent work suggests that calcium signaling could play a crucial role in the nervous system. Since calcium signals propagate considerably more slowly than electrical potentials in cells, we propose that propagating calcium waves could be a potential mechanism for facilitation. Also, calcium signaling is present in many kinds of cells including neurons and astrocytes.

9. BACKGROUND

Calcium waves are seen in both glia cells and neurons, and since we are considering both the cells as possible building block for our models, in this section we will give brief background about neurons and glia cells and how calcium signals are triggered and transmitted in them.

9.1. Glial Cells:

Glial cells or simply glia were discovered in 1856 by the pathologist Rudolf Virchow in his search for a “connective tissue” in the brain. Glial cells, also called as Neuroglia, are non-neuronal cells that plays a very crucial role in central and peripheral nervous system. The term “Glia” comes from the Greek and implies these cells are the “glue” of the nervous system. They initially got this name, because they seem to fill spaces between neurons to hold them together.

There are different types of glial cells in the central nervous system. Glial cells include oligodendrocytes, astrocytes, ependymal cells and microglia, and in the peripheral nervous system glial cells include Schwann cells and satellite cells.

For over a century, it was believed that the glia did not play any role in neural signal processing. However, with improved techniques, researchers have found out that glia cells do have an important role to play in assisting/ supporting the neurons to form synaptic connections between each other or possibly between neurons and glia cells themselves.

Out of different types of glial cells, the most abundant type of cells in the vertebrate central nervous system are Astrocytes. They constitute up to 40% of all glia cells. Astrocytes are star shaped glia

cells and are found in proximity to neurons. Astrocyte-like glial cells are also found in the nervous systems of insects [26].

Astrocytes are not electrically excitable, unlike neurons. However, they do display a form of excitation that is based on variation of Ca^{2+} concentration in cytosol. Localized changes (increase or decrease) in concentration of Ca^{2+} can propagate in the form of a wave like pattern, which is called a calcium wave. In the last decade, studies in vertebrates has shown that astrocytes propagate intra- and intercellular calcium waves in response to stimulation. The waves can be transmitted over tens of μm because of regenerative mechanisms that are present in astrocytes.

9.2. Neurons:

A neuron, also known as a nerve cell, is an electrically excitable cell that communicates with other cells via specialized connections called synapse. It is the primary component of nervous system, along with the glial cells.

Neurons are typically classified into three types based on their function. Sensory neurons respond to stimuli such as touch, sound, or light that affects the cells of the sensory organs. Motor neurons send signals from brain and spinal cord to control effectors such as muscles. Interneurons connects neurons to other neurons within the same region of the brain.

Most neurons consist of three parts: a cell body, dendrites, and a single axon. The cell body is usually compact and axon and dendrites are filaments that extrude from it. Dendrites are usually tens to a few hundred micrometers in length and axon can be as long as 1 meter in humans and other vertebrate species. The function of the axon is usually regarded as transmitting the neural output over some distance to other, target neurons. However, many interneurons that process signals locally do not have clearly defined axons. We model a neural network for facilitation that is composed of such neurons.

The signaling process in neurons is partly electrical and partly chemical. Neurons are normally polarized to a negative potential with respect to the extracellular space; the signaling potentials are typically depolarizing if they are excitatory. However, some inputs can generate hyperpolarization too. Once a neuron has been excited (by stimulus) until threshold membrane potential is reached, it then generates an action potential that can travel through the length of the cell. This is ‘electro’ part of the electrochemical. Once the electric signal reaches the axon terminal at the end of the cell, or in some cases the dendrites, it triggers the release of certain chemical messengers, also known as neurotransmitters. This is ‘chemical’ part of electrochemical. These neurotransmitters allow one neuron to communicate with another. There is another type of signal called graded potentials but that these may not reach as far as action potentials.

Calcium (Ca^{2+}) is a ubiquitous second messenger for many physiological roles. It is of critical importance to neurons, as it governs the release of neurotransmitters and thus plays a role in the transmission of signals between neurons [4].

9.3. Ca Signaling/ Wave:

A calcium wave is defined as a moving, localized increase in cytosolic Ca^{2+} , which in many vertebrate neurons and astrocytes may be followed by a succession of similar events in a periodic wave-like fashion. These Ca waves can be restricted to one cell (intracellular) or transmitted to neighboring cells (intercellular), which we are considering. The cellular and molecular mechanisms involved in the triggering, propagation, and transmission of Ca^{2+} waves have by this point have been the subject of a number of research efforts. In this section, we will give background about these mechanisms in both astrocytes and neurons.

9.3.1. Triggering Calcium Waves in Astrocytes:

The mechanism by which intracellular Ca^{2+} waves are initiated in astrocytes involves the release of neurotransmitters onto the astrocytes which leads to a chain of reactions in the following order: activation of G-protein-coupled receptors (GPCR), which in turn activates phospholipase C (PLC), and this PLC cleaves Phosphatidylinositol 4, 5 bisphosphate (PIP2) into Inositol trisphosphate (IP₃) & Diacylglycerol (DAG). DAG is converted to Arachidonic Acid (AA) which activates ARC receptors, allowing initial calcium influx into the cell. IP₃ produced in previous step diffuses to Inositol trisphosphate receptors (IP₃R) present on endoplasmic reticulum (ER) membrane, leading to activation of IP₃R channels, which allow calcium to flow out of ER [19, 11]. This initial influx of calcium ions is what triggers calcium waves.

9.3.2. Propagation of Calcium Waves in Astrocytes:

Calcium waves are spatially and temporally complex events involving many Ca^{2+} release sites (receptor channels), which then propagate throughout the cell by an amplification mechanism. Once triggered, intracellular Ca^{2+} waves can be transmitted to neighboring cells. Propagation of calcium waves in astrocytes involves lateral diffusion of calcium and trans-membrane transport via successively activated InP3 receptor channels. The law governing lateral Ca^{2+} transport is provided by Fick's first law diffusion.

9.3.3. Transmission of Calcium Waves between Astrocytes:

Transmission is the passage of a wave from one cell to the next and since we are assuming a network of cells model, this is a critical part of our model. In astrocytes, intercellular transmission of calcium waves may be mediated both by release of transmitter substances (gliotransmitters) and gap junction interconnections. In this project we are not simulating gliotransmitters, rather we are modeling gap junctions for intercellular transmission. Gap junctions are connections between cells, that directly allow ions/ molecules to pass through a regulated gate between cells. We model transmission of InP3 through gap junctions between cells and not of calcium ions. There is only weak evidence suggesting that calcium ions can pass through gap junctions, such that gap junctions have at best very low permeability to calcium [18].

9.3.4. Triggering Calcium Waves in Neurons:

The mechanisms responsible for regulating and triggering calcium waves in neurons are well established [20]. Fundamentally, calcium waves in neurons are triggered by synaptic input that activates post-synaptic channels which happen to let calcium ions in. The N-methyl-D-aspartate (NMDA) receptor, is one class of receptor whose channels conduct a significant proportion of calcium ions.

The synaptic signaling sequence between cells works in following order: pre-synaptically, depolarization (such as caused by an arriving action potential) causes voltage-operated calcium channels to open in the pre-synaptic area, and the influx of calcium causes the release of neurotransmitter. The neurotransmitter diffuses to the post-synaptic cell and activates receptors (either directly or through 2nd messengers) whose channels let in ions of some type. These can cause depolarization, or hyperpolarization, depending on the type.

9.3.5. Propagation of Calcium Waves in Neurons:

Propagation of calcium waves in neurons involves lateral diffusion of calcium, given by diffusion equation, and trans-membrane transport via RyR receptors channels as well as calcium pumps.

9.3.6. Transmission of Calcium Waves between Neurons:

Transmission of calcium waves between neurons is not modeled here. Work in this Thesis is only limited to wave propagation in neural dendrites. The issue is that depolarization would typically be caused by calcium influx, and this electrical signal would be expected to travel rapidly and cause the neuron to output, so why would not that be happening in these cells? Why would the input-output relationship in these cells be governed just by calcium waves? These questions will be addressed in the future efforts by other students.

10. MODELS FOR CALCIUM WAVE PROPAGATION

In the project supporting this MS research, we propose three candidates for biophysically-plausible substrates to model propagating facilitation: 1) a network of glial cells in which the signal is carried by calcium ions, with lateral transport by diffusion, and waves that are propagated with a regenerative positive feedback mechanism; 2) a network of neurons in which the signal is similarly carried by calcium ions, with similar wave-like propagation; and 3) a network of small neurons in which propagating electrical signals are delayed frequently by the presence of excitatory synapses with slow kinetics. This MS project is focused on the first and second candidate mechanism, and based on modeling 1) cellular processes, or “dendrites, and 2) networks of cells, in which calcium waves are the primary signaling mechanism.

There are 3 classes of processes that affect time- and spatially-varying calcium levels in a cell; 1.) lateral diffusion 2.) trans-membrane calcium transport and 3.) reactions that produce or consume calcium (e.g. buffering process).

10.1. Lateral calcium transport by diffusion in a dendrite:

Calcium waves propagate laterally in dendrites (in astrocytes and neurons) by diffusion. Since, these processes (dendrites) are thin-long one-dimensional tube like structure, we are modeling diffusion in 1D as compared to 2D or 3D. We model the lateral transport of calcium during the propagation of calcium waves using a one-dimensional version of Fick’s law (the diffusion equation), which can be represented as:

$$\frac{\partial}{\partial t} [Ca^{2+}] = D_{ca} \frac{\partial^2}{\partial x^2} [Ca^{2+}] + j_{ca} \quad 1$$

where, $[Ca^{2+}]$ is concentration of calcium ions, $\frac{\partial}{\partial t} [Ca^{2+}]$ is the local time rate of change in calcium ion concentration, and D_{Ca} is Ca diffusion coefficient. J_{Ca} represents the rate of change of the molarity of Ca in a local volume of a dendrite.

10.2. Model for calcium dynamics in astrocytes:

In the following section we introduce our models for calcium transport mechanism, pumps, different chemical reactions and components that contribute to j_{Ca} in the astrocytes model. Most of the model components discussed in below sections have rate constants associated with them which are scaled by a time increment Δt for purposes of temporal integration.

In our astrocyte model, we are not distinguishing the Endoplasmic reticulum (ER) and extra-cellular space, we just call them stores of calcium and they are assumed to have high concentration of calcium as compared to cytosolic calcium concentration present inside the cell. The small influx of calcium that we get into cytosol is assumed not to change the difference, so that the difference between the two concentrations is assumed to be constant.

10.2.1. Trans-membrane calcium transport model for astrocytes:

Figure 4 shows the complete trans-membrane calcium dynamics model for astrocytes in our model, in quasi-kinetic form. We also include calcium buffering by Calbindin in this diagram, since, like the transmembrane calcium fluxes, it is computed locally. The positive feedback loop for calcium entry into the cytosol can be described as follows: Neural input (presumably glutamate release) trigger the G-protein activation, that cleaves Phosphatidylinositol 4, 5 bisphosphate (PIP₂) into InP3 and DAG. InP3 is the 2nd messenger, which then opens InP3 receptor channels that leads to influx of calcium ions from stores. Presence of Ca^{2+} ions also have positive influence on InP3 channel opening as shown in Figure 4. So, this production of InP3 and Ca^{2+} forms a positive-feedback loop; the positive-feedback episode is terminated by reduction of open probability of the InP3 receptor, which reduces the loop gain to less than unity.

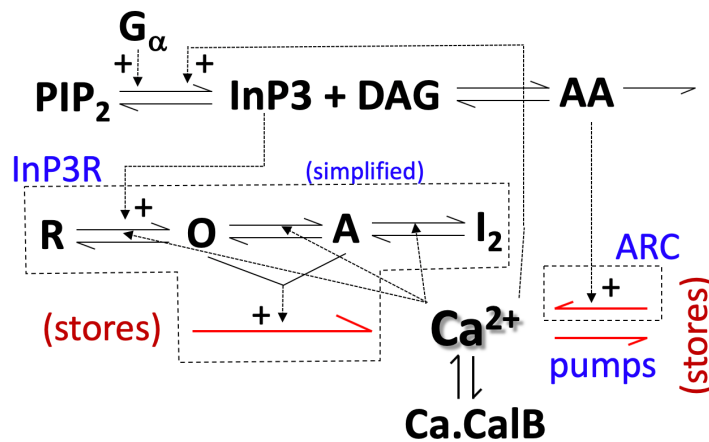


Figure 4: Trans-membrane calcium transport model for astrocytes. The buffering action of Calbindin (*CalB*) is also included for completeness, since (like membrane transport) it is modeled locally in space. Black arrows (\rightleftharpoons) represent reaction pathways, each with an associated rate constant, in conventional notation for chemical reactions, whereas red arrows (\rightleftharpoons) represent pathways for flow of calcium into and

out of Ca^{2+} stores. Dotted lines and arrows indicate an influence of a given molecule/chemical on a reaction or on the opening of an ion channel; and a + sign represents a positive influence on a reaction rate or channel opening. InP3R indicates the InP3 receptor, and R, O, A and I₂ are different states for this receptor's calcium channels. ARC represent Arachidonate-regulated calcium channels. Figure courtesy of Patrick Shoemaker.

The Arachidonate-regulated calcium (ARC) channels have high Ca^{2+} selectivity and are activated by Arachidonic acid (AA). ARC channels are the source of initial calcium entry into the cytosol from stores. Calcium pumps like (SERCA pumps; introduced below) and other sequestration mechanisms are responsible for removing calcium from the cytosol. As the Ca^{2+} diffuses in the cytosol, it can encounter high-affinity Ca^{2+} -binding proteins / substances, such as Calbindin-D_{28k} (CalB) that act as cytosolic Ca^{2+} buffers. These Ca^{2+} -buffers act as modulators of short-lived intracellular Ca^{2+} signals; they affect both the temporal and spatial aspects of these transient increases in Ca^{2+} .

10.2.2. InP3 receptor kinetics:

The InP3 receptors that mediate positive feedback are critical for calcium wave propagation. Their properties are quite complex (in fact, they have been characterized as ‘bizarre’ in reviews (Dawson, 1997)). We have chosen to implement a model for the receptor kinetics that derives from a 10-state model that collapses into 6 states with the introduction of state-dependent rate functions [15].

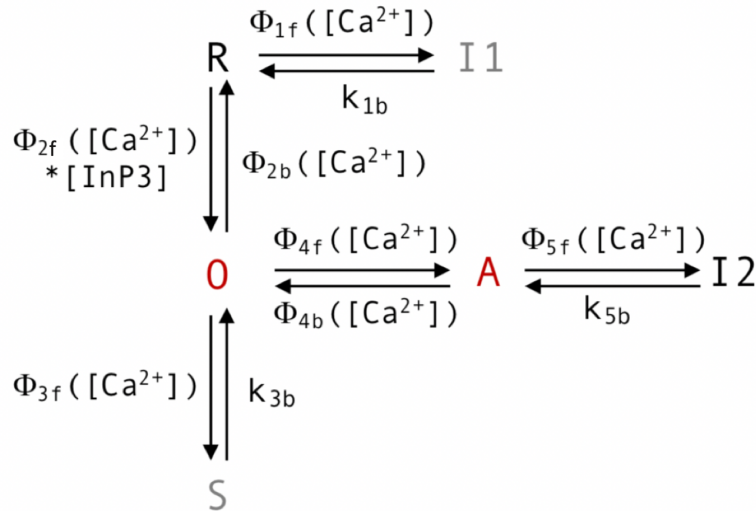


Figure 5: The Sneyd-Dufour model for InP3 receptor kinetics. Opening of the receptor's calcium channel is associated with states O and A. The functions denoted by ϕ are calcium-dependent rate functions. Transition from the native state R to O involves binding of the ligand InP3, reflected by its presence as a factor in the rate for that transition. The states rendered in gray, I1 and S, were found to have little participation in receptor function under the conditions we simulated, and are not included in our models. This kinetic structure is associated with each of the four subunits of the complete receptor.

In terms of channel open probability, the state O corresponds to ‘weakly open’ and A to ‘strongly open’. The states rendered in gray, I1 and S (in Figure 5), were found to have little participation in

receptor function under the conditions we simulated, and are not included in our models. InP3 receptors consist of four independent and identical subunits and allows Ca^{2+} current when all four subunits are in state O, or all four are in state A, or some intermediate combination (for instance, when three are in state O, and one is in state A) [15]. We assume that the more subunits there are in state A, the greater the open probability of the receptor. With these assumptions, the open probability of the receptor is thus $(0.1 * O + 0.9 * A)^4$ [15]. When InP3 concentration is stepped, the time-course of the distribution of the subunits among the states leads to a brief period of high open probability followed by much lower open probability. This feature is essential to the formation of calcium waves in cells incorporating the InP3 receptor.

The calcium influx through InP3 receptor channels is given by an expression of the form:

$$j_{InP3} = k_{Ca} * Open_{InP3} \quad 2$$

where, k_{Ca} is the calcium influx rate constant for open InP3 channels, and is proportional to the InP3 receptor density in the ER and/or plasma membranes. $Open_{InP3}$ is probability of open states in InP3 channels. $Open_{InP3}$ is modeled according to [15] and can be calculated from the sum of the two open states, O and A , in the system of ordinary differential equations (given below).

$$Open_{InP3} = (f_O * O + f_A * A)^4 \quad 3$$

where, f_O and f_A are relative dependence of open probability on O and A states.

The InP3 channels states are calculated as follows;

$$r_{O \rightarrow R} = f_{2ba} ([\text{Ca}^{2+}])$$

$$r_{R \rightarrow O} = f_{2fa} ([\text{Ca}^{2+}] * [\text{InP}_3])$$

$$r_{O \rightarrow A} = f_{4fa} ([\text{Ca}^{2+}])$$

$$r_{A \rightarrow O} = f_{4ba} ([\text{Ca}^{2+}])$$

$$r_{A \rightarrow I_2} = f_{5fa} ([\text{Ca}^{2+}])$$

$$r_{I_2 \rightarrow A} = r_{5b}$$

$$\frac{dR}{dt} = (r_{O \rightarrow R} * O) - (r_{R \rightarrow O} * R)$$

$$\frac{dO}{dt} = (r_{R \rightarrow O} * R) + (r_{A \rightarrow O} * A) - ((r_{O \rightarrow R} * O) + (r_{O \rightarrow A} * O))$$

$$\frac{dA}{dt} = (r_{O \rightarrow A} * O) + (r_{I_2 \rightarrow A} * I_2) - ((r_{A \rightarrow O} * A) + (r_{A \rightarrow I_2} * A))$$

$$\frac{dI_2}{dt} = (r_{A \rightarrow I_2} * A) - (r_{I_2 \rightarrow A} * I_2)$$

where $r_{5b}, f_{2ba}, f_{2fa}, f_{4fa}, f_{4ba}, f_{5fa}$ are InP3 receptor states rate functions of calcium concentration $[Ca^{2+}]$ as shown in Figure 5. We compute these functions using equations shown below, where Ca is calcium concentration in μM and other rate and channel constant values are taken from Table 1.

$$f_{1fA} = \frac{(k1f * L1 + l2f)}{L1 + (1 + \frac{L1}{L3})} * Ca \quad 4$$

$$f_{2fA} = \frac{(k2f * L3 + l4f * Ca)}{L3 + (1 + \frac{L1}{L3})} * Ca \quad 5$$

$$f_{2bA} = \frac{(k2b + l4b * Ca)}{\left(1 + \frac{Ca}{L5}\right)} \quad 6$$

$$f_{3fA} = \frac{(k3f * L5)}{(L5 + Ca)} \quad 7$$

$$f_{4fA} = \frac{(k3f * L5 + l6f) * Ca}{(L5 + Ca)} \quad 8$$

$$f_{4bA} = \frac{(k4b + l6b) * L1}{(L1 + Ca)} \quad 9$$

$$f_{5bA} = \frac{(k1f * L1 + l2f) * Ca}{(L1 + Ca)} \quad 10$$

10.2.3. Models for PIP2 – InP3 – DAG – AA Signaling Cascade:

Binding of a signaling molecule to a G protein-coupled receptor (GPCR) results in G protein activation, which in turn triggers the production of second messengers. The effector enzymes in this cascade is Phospholipase C (PLC). This PLC cleaves Phosphatidylinositol 4,5-bisphosphate (PIP2) into IP3 (inositol triphosphate) and DAG (diacylglycerol). IP3 diffuses over to ER (Endoplasmic Reticulum) and it binds with calcium ion channel and it allows calcium ions (Ca^{2+}) to flow from inside of the ER to the cytosol. And some of the DAG along with Ca^{2+} ions works together to activate PKC, which adds phosphates to target protein which triggers the cellular response. Also, studies of the DAG/protein kinase C (PKC) pathway indicate that PKC is involved

in the termination of astrocytic Ca^{2+} transients [23, 24, 25]. Equations given below show clearly that PKC has an inhibitory effect on InP3 production – but we found when looking at the experimental results that this effect is minimal, so we left it out of the Figure 4.

Accordingly, equations for InP3, AA and PKCv updates are as following:

$$\frac{d\text{InP}_3}{dt} = \frac{G_{in} + kd_{1f} * Ca}{1 + k_{i2} * PKC_v} - k_{1b} * \text{InP}_3 \quad 11$$

$$\frac{dAA}{dt} = k_{1b} * \text{InP}_3 - k_{1b} * AA \quad 12$$

$$\frac{dPKC_v}{dt} = k_{4f} * Ca * (PKC_0 - PKC_v) - k_{4b} * PKC_v \quad 13$$

where parameters and rate constants used are defined in the Table 1 and G_{in} represents the local concentration of G-protein.

10.2.4. Models for Calcium Pumps:

The models for pumps are taken from [14] and are adapted to account for efflux from plasma membrane Ca^{2+} -ATPase pumps (PMCA) and $\text{Na}^+/\text{Ca}^{2+}$ exchanger pumps (NCX), which are seen in Glia cells [22].

The calcium flow associated with pumps is described by a combination of first order Hill's equation that corresponds to plasma membrane pumps and second order Hill's equation that corresponds to SERCA pumps, respectively.

$$j_{pumps} = k_p^1 * \left(\frac{C_s}{(k_{pc}^1 + C_s)} \right) + k_p^2 * \left(\frac{C_s^2}{(k_{pc}^2 + C_s^2)} \right) \quad 14$$

where k_p^1 , k_p^2 , k_{pc}^1 and k_{pc}^2 are calcium 1st- and 2nd-order pump constants, C_s is cytosolic calcium concentration, and j_{pumps} is calcium efflux due to pumps.

10.2.5. Model for Ca Buffering:

Calcium buffering can be described as an “uptake and release” of free calcium in cytosol by Ca^{2+} -binding proteins (e.g., Calbindin-D_{28k}). We model all such buffering by a single reaction. This mechanism is described as a reversible reaction given by:



As the Ca^{2+} diffuses in the cytosol, free Ca^{2+} binds (reacts) with CalB, that acts as cytosolic Ca^{2+} -buffers. This bounded Ca^{2+} is released back into cytosol by the reverse reaction.

The equations for calbindin and cytosolic calcium are given by:

$$j_{sfb} = k_{c_{bf}} * C_s * ([\text{CalB}0] - [\text{Ca.CalB}]) \quad 15$$

$$j_{sb_f} = k_{c_{bb}} * [\text{Ca.CalB}] \quad 16$$

$$\frac{dC_s}{dt} = j_{sb_f} - j_{sfb} \quad 17$$

$$\frac{d[\text{Ca.CalB}]}{dt} = j_{sfb} - j_{sb_f} \quad 18$$

where $k_{c_{bf}}$ and $k_{c_{bb}}$ are rates for calcium buffering, with baseline calbindin being, $[\text{CalB}0] = 40 \mu\text{M}$. C_s and $[\text{Ca.CalB}]$ is cytosolic and bounded calcium concentration, respectively. Here we use “flux” symbols j_{sb_f} and j_{sfb} for rates of change in unbound and bound calcium concentrations, respectively, for consistency with the kinetic formalism.

10.2.6. Model for Gap Junctions:

Gap junctions are a specialized intercellular connection between cells (either astrocytes or neurons). They directly connect the cytoplasm of two cells, which allows various molecules, ions and electrical impulses to directly pass through a regulated gate between cells. In vertebrate astrocytes, evidence suggests that there is direct exchange of InP3 and Ca^{2+} through gap junction-like interconnections between cells. But as per [18], calcium flow through gap junctions seems to be extremely limited, so we are ignoring it in our model and thus we only model the direct exchange of InP3.

The influx or efflux of InP3 through gap junctions is modeled by the following equation:

$$j_{Gap} = r_{inp3} * ([InP3_{c1}] - [InP3_{c2}]) \quad 19$$

where r_{inp3} is the rate constant for flow of calcium between cells through gap junctions and j_{Gap} is the flow of InP3 from cell 1 into cell 2, and this is positive if concentration is higher in cell 1, and negative if concentration is higher in cell 2.

10.2.7. Model for leakage:

The influx of calcium per unit area of plasma membrane due to leakage mechanism is assumed to be constant, because the difference in calcium concentration between cytosolic and external calcium is assumed to be nearly constant, due to the much higher calcium levels in the external space. Leakage flux is given by following equation:

$$j_{leakage} = k_{lk} \quad 20$$

where k_{lk} is calcium leakage rate in $\mu\text{M}/\text{S}$.

10.2.8. Model for ARC Channels:

Unlike store-operated channels (activation of which is, dependent on the depletion of internal Ca^{2+} stores, notably the endoplasmic reticulum (ER)), Arachidonate-regulated Ca^{2+} (ARC) channels specifically depend on the receptor-mediated generation of low levels of intracellular arachidonic acid [21].

In our model, ARC channels are only responsible for initial influx flow of calcium. The calcium influx through ARC channels is given by following equations:

$$j_{ARC} = k_{aa} * AA \quad 21$$

where k_{aa} is the calcium influx rate for open ARC channels and AA is concentration of arachidonic acid.

10.2.9. Parameters and Constants associated with Astrocyte Model:

This section introduces all the parameters and constants that govern models of the astrocyte that we have formulated for simulation and analysis in section 10.2.1 – 10.2.8.

Parameter / Constant	Nominal Value	Units	Definition
DCa	240	$\mu\text{m}^2.\text{s}^{-1}$	Ca diffusion coefficient in astrocytes
fCa	0.3	-	Fraction to reduce DCa due to intracellular crowding
$DInP3$	300	$\mu\text{m}^2.\text{s}^{-1}$	InP3 diffusion coefficient in astrocytes
$fInP3$	0.7	-	Fraction to reduce DInP3 due to intracellular crowding
kGI	40	$\mu\text{M}.\text{s}^{-1}$	Rate of InP3 production induced by glutamatergic input
$kdIf$	6	$\mu\text{M}.\text{s}^{-1}$	Rate constant for $[\text{Ca}]$ -dependent production of InP_3
$kcbf$	0.7	$\mu\text{M}^{-1}.\text{s}^{-1}$	Rates for calcium buffering
$kccb$	10	s^{-1}	Rates for calcium buffering
kCa	600	$\mu\text{M}.\text{s}^{-1}$	Calcium influx rate constant for open InP3R channels
kaa	6	$\mu\text{M}^2.\text{s}^{-1}$	Calcium influx rate for open ARC channels
kGI	40	$\mu\text{M}.\text{s}^{-1}$	rate of InP3 production induced by glutamatergic input
$rinp3$	500	$\mu\text{M}.\text{s}^{-1}$	Rate constants at interconnections/ gap junctions
$ki2$	0.0943	μM^{-1}	for inhibition of InP3 production by PKC
$k4f$	0.6	$\text{s}^{-1}.\mu\text{M}^{-1}$	Rate constant for activation of PKC
$k4b$	0.5	s^{-1}	Rate constant for deactivation of PKC
PKC_0	1	μM	Available concentration of PKC
$kp1$	75	$\mu\text{M}.\text{s}^{-1}$	Calcium 1st-order pump constants
$kp1c$	1.8	μM	Calcium 1st-order pump constants
$kp2$	12	$\mu\text{M}.\text{s}^{-1}$	Calcium 2nd-order pump constants
$kp2c$	0.10	μM	Calcium 2nd-order pump constants
$K1k$	1	$\mu\text{M}.\text{s}^{-1}$	Calcium leakage rate
$k1b$	2.5	$\mu\text{M}.\text{s}^{-1}$	For conversion of InP3 into AA (and then back into PIP2)

$k1f$	0.640	$s^{-1} \cdot \mu M^{-1}$	Constant associated InP3R rate functions
$k1b$	0.040	s^{-1}	Constant associated InP3R rate functions
$k2f$	37.40	$s^{-1} \cdot \mu M^{-1}$	Constant associated InP3R rate functions
$k2b$	1.400	s^{-1}	Constant associated InP3R rate functions
$k3f$	0.110	s^{-1}	Constant associated InP3R rate functions
$k3b$	29.80	s^{-1}	Constant associated InP3R rate functions
$k4f$	4.000	$s^{-1} \cdot \mu M^{-1}$	Constant associated InP3R rate functions
$k4b$	0.540	s^{-1}	Constant associated InP3R rate functions
$L1$	0.120	μM	Constant associated InP3R rate functions
$L3$	0.025	μM	Constant associated InP3R rate functions
$L5$	57.40	μM	Constant associated InP3R rate functions
$l2f$	1.700	s^{-1}	Constant associated InP3R rate functions
$l2b$	0.800	s^{-1}	Constant associated InP3R rate functions
$l4f$	1.700	$s^{-1} \cdot \mu M^{-1}$	Constant associated InP3R rate functions
$l4b$	2.500	s^{-1}	Constant associated InP3R rate functions
$l6f$	4707	s^{-1}	Constant associated InP3R rate functions
$l6b$	11.40	s^{-1}	Constant associated InP3R rate functions
$r1b$	0.840	s^{-1}	Rate constants associated with the state-dependent InP3R model
$r3b$	29.80	s^{-1}	Rate constants associated with the state-dependent InP3R model
$r5b$	0.840	s^{-1}	Rate constants associated with the state-dependent InP3R model

Table 1: List of parameters and constants associated with Astrocyte Model. Parameters that are shown in red color are varied in our experiments, while others are fixed at give values. ‘-’ in units column represents unitless parameter value. All parameters and constants associated with InP3 rate functions are referred from [15].

10.3. Models for calcium dynamics in neurons:

In the following section, we introduce calcium transport model for neurons, which includes RyR channels, and different calcium pumps.

10.3.1. Trans-membrane calcium transport model for neurons:

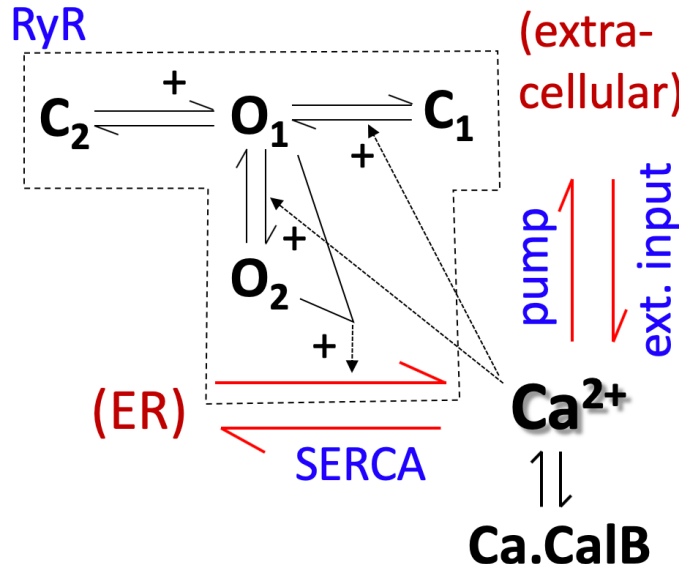


Figure 6: Trans-membrane calcium transport model for neurons. Buffering of calcium by Calbindin is again included for completeness. \rightleftharpoons (in black color) represents reversible reactions and \rightleftharpoons (in red color) represents flow of calcium in and out of cell (and ER) by external input and pumps (SERCA and plasma membrane pumps) respectively, + sign represents positive influence on the reaction, dotted arrow represents influence of a given molecule/chemical on the reaction. C_2 , O_1 , C_1 and O_2 are different states for RyR receptor's calcium channels. Figure courtesy of Patrick Shoemaker.

The figure above shows the complete trans-membrane calcium dynamics model for neurons in our model, in quasi-kinetic form. Again we include calcium buffering by Calbindin. The positive feedback loop for calcium entry into the cytosol can be described as follows: Neural input in the form of calcium influx (e.g., through NMDAR's). This influx of calcium opens RyR channels. RyR channels have calcium dependent kinetics like InP3 channels described in astrocyte model, leading to influx of more calcium from ER stores, which in response opens more RyR channels. The positive-feedback loop is limited/ terminated by nonlinear calcium pumps (SERCA and plasma membrane) and other sequestration mechanisms that remove calcium from the cytosol.

10.3.2. Model for Ryanodine receptor (RyRs):

The calcium flux density through ryanodine receptor channels in the ER membrane is given by an expression of the form:

$$j_R = r_{Ca} * Open_{RyR} * (C_e - C_s)$$

where, r_{Ca} is the calcium influx density for open RyR channels, C_e is the calcium concentration in endoplasmic reticulum, and C_s is cytosolic calcium.

The $Open_{RyR}$ is the open probability for open RyR channels and is modeled according to [16]. It can be calculated as the sum of the two open states, O_1 and O_2 determined by the system of ordinary differential equations (given below), emerging from a four-state Markov model with kinetic constants $k_a^-, k_a^+, k_b^+, k_b^-, k_c^+, k_c^-$.

$$\begin{aligned} O_1 &= 1 - C_1 - O_2 - C_2 \\ \frac{dC_1}{dt} &= k_a^- * O_1 - k_a^+ * C_c^4 * C_1 \\ \frac{dO_2}{dt} &= k_b^+ * C_c^3 * O_1 - k_b^- * O_2 \\ \frac{dC_2}{dt} &= k_c^+ * O_1 - k_c^- * C_2 \end{aligned}$$

10.3.3. Model for Pumps:

In following section we describe SERCA and Plasma membrane pumps, along with their equations.

10.3.3.1. SERCA Pumps:

The model for SERCA pumps in neurons is taken from [16] and is slightly modified from the model used for astrocytes. It remains a 2nd order Hill equation, but with the ER calcium concentration appearing in the denominator of the equation 23, because as per [16] model, ER calcium is allowed to deplete, and this has an effect on the pump rate.

$$j_{serca} = k_p^2 * \left(\frac{C_s^2}{(k_{pc} + C_s) * C_e} \right) \quad 23$$

where k_p^2 and k_{pc} are calcium 2nd-order pump constants, C_s is the cytosolic calcium concentration, C_e is the local ER calcium concentration, and j_{serca} is calcium efflux due to SERCA pumps. In accordance with the [16], ER calcium levels are *not* assumed to remain fixed, but are allowed to vary locally as calcium flows into the cytosol from the ER and vice-versa. Also, ER calcium concentration is treated as another state in the numerical model.

10.3.3.2. Plasma Membrane Pumps:

The mode for Plasma membrane pumps in neurons is taken from [16] and is expressed as first order Hill's equation:

$$j_{plasma} = k_p^1 * \left(\frac{C_s}{(k_{pc}^1 + C_s)} \right) \quad 24$$

where k_p^1 and k_{pc}^1 are calcium 1st-order pump constants, C_s is cytosolic calcium and j_{plasma} is calcium efflux due to plasma membrane pumps.

10.3.4. Model for Ca Buffering:

Model for Calcium buffering is identical to what was introduced in astrocytes section 7.2.5 and we have used the same equations as mentioned there. Refer Table 2 for parameter values.

10.3.5. Model for Gap junction:

Model for Gap junctions is identical to what was introduced in astrocytes section 7.2.6 and we have used the same equations as mentioned there. Refer Table 2 for parameter values.

10.3.6. Model for leakage:

Model for leakage is identical to that introduced in astrocytes section 7.2.7 and we have used the same equations as mentioned there. Refer Table 2 for parameter values.

10.3.7. Parameters and Constants associated with Astrocyte Model:

This section introduces all the parameters and constants that govern models of the neurons that we have formulated for simulation and analysis in section 10.3.1 – 10.3.6.

Parameter / Constants	Value	Units	Definition
DCa	240	$\mu\text{m}^2.\text{s}^{-1}$	Ca diffusion coefficient in neurons
fCa	1	-	fraction to reduce DCa due to intracellular crowding
DInP3	300	$\mu\text{m}^2.\text{s}^{-1}$	InP3 diffusion coefficient in neurons
rCa	600	μM^{-2}	Calcium influx rate constant for open RyR channels
kp1	75	$\mu\text{M}.\text{s}^{-1}$	Calcium 1 st -order pump constants
kpc1	1.8	μM	Calcium 1 st -order pump constants
kp2	4400	$\mu\text{M}.\text{s}^{-1}$	Calcium 2 nd -order pump constants
kp2c	0.10	μM	Calcium 2 nd -order pump constants
K1k	1.5	$\mu\text{M}.\text{s}^{-1}$	Calcium leakage rate
kcbf	0.7	$\mu\text{M}.\text{s}^{-1}$	Rates for calcium buffering
kccb	10	s^{-1}	Rates for calcium buffering
CalB0	40	μM	Available Calbindin concentration
kAneg	28.8	s^{-1}	RyR receptor state rates
kApos	1500	$\mu\text{M}^{-4}.\text{s}^{-1}$	RyR receptor state rates
kBneg	385.9	s^{-1}	RyR receptor state rates
kBpos	1500	$\mu\text{M}^{-3}.\text{s}^{-1}$	RyR receptor state rates
kCpos	1.75	s^{-1}	RyR receptor state rates
kCneg	0.1	s^{-1}	RyR receptor state rates
VolR	50	-	Volume Ratio, Cytosol to ER

2: List of parameters and constants associated with Neuron Model. Parameters that are shown in red color are varied in our experiments, while others are fixed at give values. ‘-’ in units column represents unitless parameter value.

11. MORPHOLOGICAL STRUCTURE OF CELLS

Astrocytes are star-shaped cells that have radiating cellular processes that we will refer to as ‘dendrites’ for simplicity (even though ‘dendrite’ is usually used to refer to a form of neural process). For modeling astrocytes and neurons, we have built 3 morphological units; cell body, straight and branched dendrite, that combined together forms a generic “cell” and can represent an astrocyte (or even neuron). The dendritic length is the same from base to tip for either straight or branched dendrites and the dendritic diameter is assumed to be $1\mu\text{m}$.

All three subunits are composed of compartments, which can be regarded as defining discrete finite elements or a *grid* for our signal propagation model. The distance between two compartments is (assumed to be) equal to $1\mu\text{m}$. The cell body is itself a single compartment, whose total cross-sectional area is assumed to be 12 times that of a single dendrite at the junction point. Straight dendrites are made of 10 compartments each and every cell has 8 straight dendrites (see Figure 7). Therefore, every straight dendrite is $10\mu\text{m}$ long (but we have also experimented with longer dendrites as well. For e.g. $100\mu\text{m}$ long dendrites). Branched dendrites are made of 3 segments and these segments are made of 5 compartments each, and we have 4 branched dendrites in our model. Therefore, every segment in branched dendrite is $5\mu\text{m}$ long. To characterize the state of the compartments, a data structure is defined that maintains the value of required states (which include for example $[\text{Ca}^{2+}]$, $[\text{DAG}]$, $[\text{InP}_3]$, and other states for the local receptor populations).

Using these subunits, we have built different types of models for experiment (discussed in section 13.1.). We use cell body along with pair of dendrites (connected on both end) to build ‘single cell–two dendrite model’. Similarly, we can build more realistic cells with more stereotypical dendrites.

For astrocyte modeling, we built single dendrite (with no cell body), single cell with pair of dendrites, two cells with pair of dendrites each and a stereotypical cell with 12 dendrites as shown in Figure 7. Using these stereotypical cells, we have built network of cells as shown in Figure 8. For neurons, our models are limited to single dendrite (with no cell body) and single cell with pair of dendrites. We have not built any network of neurons.

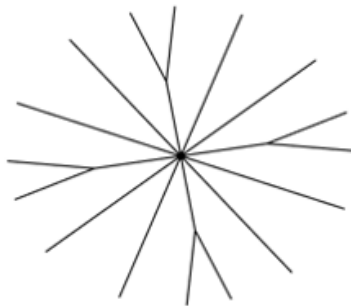


Figure 7: Single cell in our model having one cell body, eight straight dendrites, and four branched dendrites with a total of 12 dendrites.

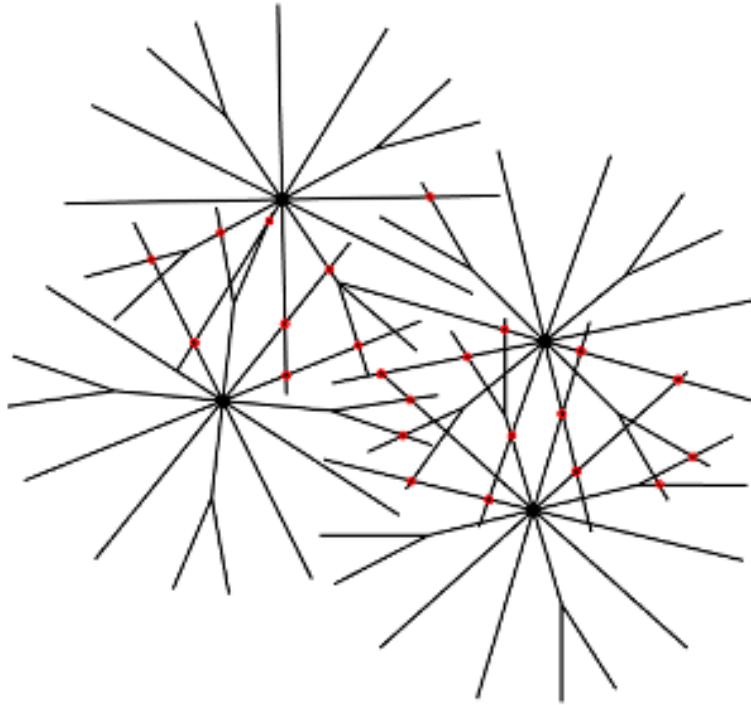


Figure 8: Four interconnected cell in our model interconnected together by gap junctions. Red dots represent gap junction interconnections.

12. NUMERICAL MODELING & SIMULATION

We simulate the propagation of calcium waves in network of cells arranged in a two-dimensional network and in individual dendrites as well. Network modeling only looks at networks of the astrocytes, and not networks of neurons. Our work on neurons is limited to dendritic propagation only. We are not clear on how calcium waves would be transmitted from neuron to neuron, although it might be either by synapses or gap junctions, and furthermore, the neural model is complicated by the fact that calcium entry typically causes depolarization as well.

All the modeling and simulations are carried out in Matlab. We have open sourced our codebase (scripts along with dependencies), which is publicly available on GitHub [29]. We generate a network of these cells with a stereotypical architecture, but with randomness introduced in their placement and orientation. Cells are placed on a hexagonal grid for symmetry, but random offsets in the x and y directions are added to the cell positions, and they are rotated randomly at placement. Below in Figure 9 you can see a skeletonized diagram of a network of 143 astrocytes interconnected to each other.

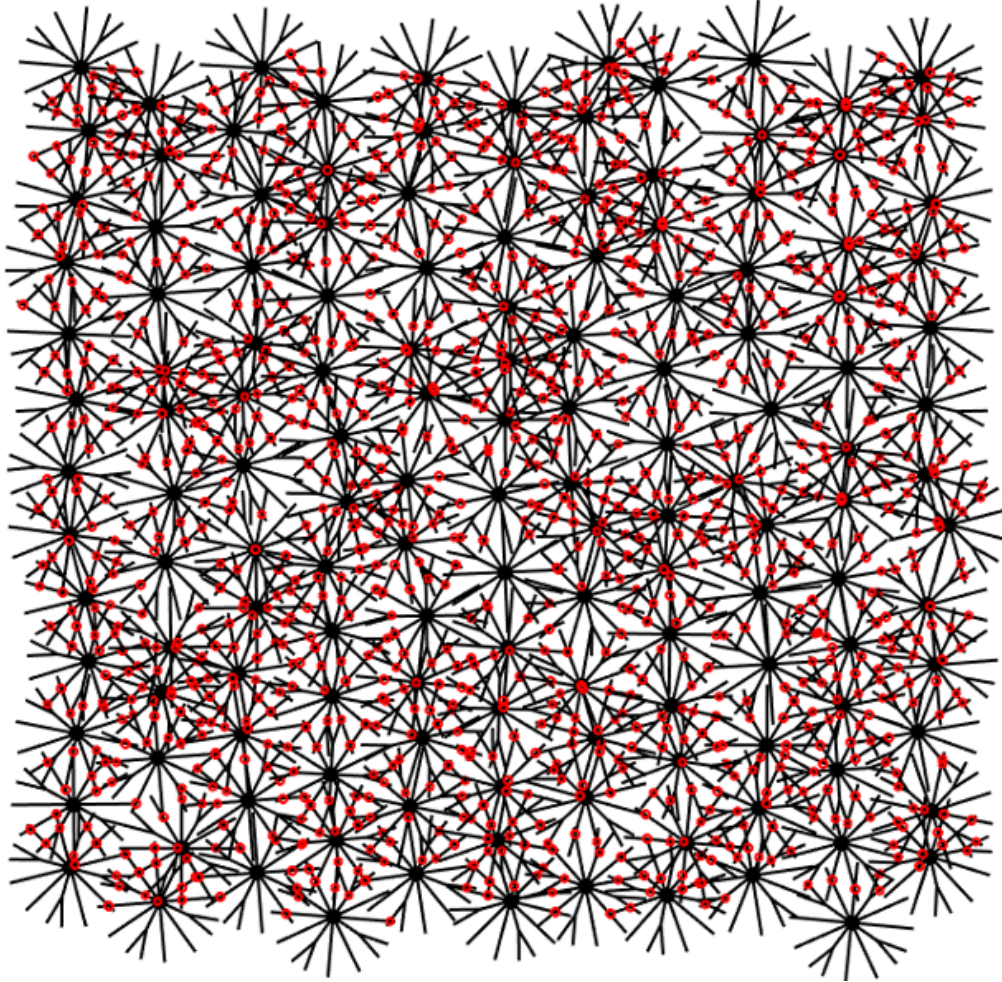


Figure 9: 2D Network of 143 astrocytes interconnected together. Red dots represent gap junction interconnections. Black dots represents cell body and black lines originating from cell body represents dendrites.

12.1. Mathematical Formulation:

Our model (dendrites and cell body) is discretized into compartments and calcium is transported laterally between compartments by diffusion, and trans-membrane calcium flux (and buffering) is calculated locally at each compartment.

We can divide the trans-membrane components of our model into two 1) Source component: refers to channels or entities that increases calcium in cytosol. (e.g. receptor channels (InP3 and RyR), leakage) and 2) Sink component: refers to entities (pumps, buffering) that decreases calcium concentration in cytosol. So, after incorporating these two components, our model equation can be written as:

$$\frac{\partial}{\partial t} [Ca^{2+}] = D_{Ca} \frac{\partial^2}{\partial x^2} [Ca^{2+}] + j_{src} - j_{snk} \quad 25$$

where, j_{src} represent source terms and j_{snk} represent sink terms.

In order to solve this equation numerically, we are using MOLE (*Mimetic Operators Library Enhanced*) library (discussed in 12.4) to do spatial integration and for temporal integration we are doing simple quadrature, i.e. multiplying the equation 25 by a finite time increment Δt and summing over time.

12.2. Numerical Solution:

We have solved our model numerically using Mimetic Discretization Methods [17]. After discretizing our spatial domain, the model can be written in matrix-vector format given by following equation;

$$U^{n+1} = L * U^n + (S_{rc} + S_{nk}) \quad 26$$

where, L is our mimetic Laplacian operator (matrix) and S_{rc} and S_{nk} are vectors that represent flux from source and sink components in our model.

We construct 1D mimetic Laplacian operator L using MOLE library. This operator returns a sparse matrix of size $(m+2)$ by $(m+1)$ is called using a command in Matlab, “*lap(k, m, dx)*”, as shown below.

$$L = \text{lap}(k, m, dx)$$

where, k is operator's order of accuracy, m is the number of cells required to attain the desired accuracy, dx is the step size along x -axis.

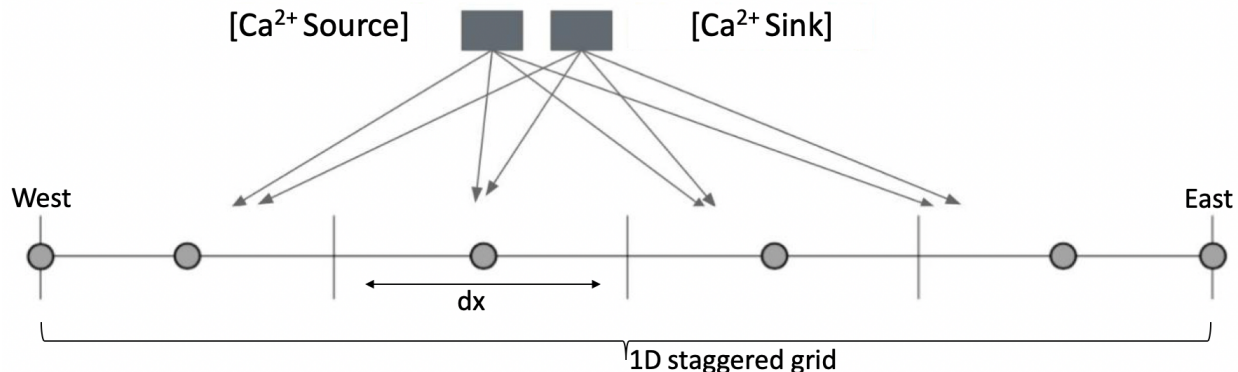


Figure 10: 1D staggered grid with Ca source and sink acting on every grid point.

Generating an array of 1D staggered grid points and storing them in “*grid*” is done in Matlab as shown below,

$$\text{grid} = [\text{west} \quad \text{west} + dx/2 : dx : \text{east} - dx/2 \quad \text{east}]$$

where, *west* and *east* are two ends of our *grid* and *dx* is the step size on x-axis. We have calcium source and sink terms acting on every grid point and it can be visualized as shown in Figure 10.

12.3. Boundary Conditions:

As per assumptions in our model, dendrites are sealed at one end (flux = 0), and the flux out at the other end must be set to match the flux into the cell body. And, similarly fluxes out of cell body on the other end must match the sum of fluxes from the dendrites. This requires a Robin boundary condition, which is a weighted combination of Dirichlet boundary conditions and Neumann boundary conditions. In MOLE library, this can be imposed using following statement:

$$BC = \text{robinBC}(k, m, dx, a, b)$$

where, k is operators order of accuracy, m is the minimum number of cells required to attain the desired accuracy, dx is the step size along x-axis, a = 0 and b = 1 are coefficients in robin boundary conditions.

12.4. MOLE Library:

MOLE (Mimetic Operators Library Enhanced) is a high quality (C++ and Matlab) library that implements high-order mimetic operators to solve partial difference equations. It provides discrete analogs of the most vector calculus operators: *Gradient*, *Divergence*, *Laplacian* and *Curl*. These operators (matrices) act on staggered grids (uniform and non-uniform) and they satisfy local and global conservation laws. The mathematics of MOLE is based on the work of Corbino & Castillo (2020) [17].

13. EXPERIMENTS:

In this section we will discuss how experiments were designed and carried out. We have done hundreds of experiments if not more to understand:

1. The dynamics of Ca waves in cellular processes, cells, and networks of cells;
2. How the parameters that are varied affect the wave speed, wave amplitude, regenerative mechanics, and damping behavior.

13.1. Design of experiments:

We can break down the experiments into following categories:

- A.) Different types of test beds:
 - a) Single dendrite.
 - b) Two dendrites connected through cell body.
 - c) Two cells connected end-to-end with two dendrites each.
 - d) Network of complete cells interconnected to each other randomly.
- B.) Varying parameters:
 - a) Changing one parameter at a time, while keeping others at their baseline value.
 - b) Changing two parameters together, while keeping others at their baseline value.

13.2. Important Parameter:

Our model contains a large number of parameters (see Table 1 and 2Table 3), but not all of them are so important physiologically for wave propagation. We have selected few parameters (shown in Table 3) based on physical intuition that will govern dynamics of calcium wave. For example, the most important parameter in our model is k_{Ca} , that corresponds to calcium influx through open InP3 channels, and is proportional to receptor density. Since, we are truly modeling InP3-mediated propagation in astrocytes, any parameter that governs InP3 ($kd1f$, k_{Ca} , $ki2$, $fInP3$) will be critical for our purposes. Similarly, we have selected other parameters as well as shown in Table 3 along with their definitions.

We selected *reference values* for these parameters, which appear to be physiologically reasonable and in combination give traveling wave behavior. We call these *reference values* as the *base line values* for each parameter. By default all parameters are set to their baseline values, unless otherwise stated.

Parameter	Definition	Baseline Values
$kd1f$	Ca-dependent production of InP3	$5 \mu\text{Ms}^{-1}$
kaa	Ca-influx rate for open ARC channels	$6 \mu\text{M}^2.\text{s}^{-1}$
f_{Ca}	Fraction to reduce DCa due to intracellular crowding	0.3
$fInP3$	Fraction to reduce DInP3 due to intracellular crowding	0.7
k_{Ca}	Calcium influx rate constants for open InP3 channels	$600 \mu\text{M}.\text{s}^{-1}$
k_{cbf}	Rates for Ca buffering	$0.7 \mu\text{M}^{-1}.\text{s}^{-1}$
k_{cbb}	Rates for Ca buffering	10s^{-1}
$ki2$	Inhibition of InP3 production by PKC	$0.0943 \mu\text{M}^{-1}$

Table 3: Model parameters and rate constants that are varied in experiments for Astrocyte model. All these parameters are also shown in Table 1; we are re-iterating these for clarity.

13.3. Characteristics examined:

We are interested in examining following characteristics or properties of calcium waves in dendrites and cells in our experiments.

13.3.1. Wave Regimes:

We are interested in exploring different regimes for calcium waves, depending on the physiological parameters shown in Table 3. Our preliminary experiments suggested that there exist three such regimes: Regenerative, Damping and Abortive. Our initial guess was that there would be different ranges of parameters that would govern these regimes. We examine and show results for these property in section 14.1.

13.3.1.1. Regenerative Regime:

In regenerative regime, calcium waves travel through the entire dendritic distances, passing through cell body and gap junctions by regenerating itself. We define a wave to be regenerative, if it is initiated in one cell and is able to reach the end of other cells (in a network) by passing through gap junctions and cell bodies. You can refer video (Figure 13) for this in Appendix B. In our experiments, we are looking at how does model parameter(s) impact the ability of a wave to regenerate itself, reflected in its ability to propagate for long distance, before it dies out (if it does)?

13.3.1.2. Damping Regime:

In damping regime, calcium waves gets damped as it propagates and die before it reaches till the end of cell or dendrite. We define a wave to be damping, if a propagating wave, which was initiated say on the left end of cell (or left dendrite), dies before it reaches the other end of the cell (or dendrite). Damping waves are characterized by (decrease) reduction in wave amplitude as it propagates and eventually dies. You can refer video (Figure 14) for this in Appendix B. In our experiments, we are looking at does a parameter(s) influence damping of a wave, i.e., a decrease in amplitude of the wave as it propagates?

13.3.1.3. Abortive Regime:

We further observe that abortive regime exist, where our model is not able to generate waves that could propagate even a few micrometers. Typically, in abortive regime a wave or calcium bump is never able to cross the cell body or the dendritic distance. You can refer video (Figure 15) for this in Appendix B.

13.3.2. Wave speed:

Wave speed is the single most important property that we are interested in and from our research [6], we know the speed at which facilitation propagates. In our experiments, we examine what is range of (low-high) speed that we can get? Does wave speed increase or decrease with change in a parameter values?

13.3.3. Wave amplitude:

Does amplitude of wave increase, decrease or remain unchanged with change in a parameter value?

13.3.4. Region of influence:

Does given parameter have local or global effect in our model? A parameter having local influence will affect wave properties locally, whereas, a parameter having global influence will affect the wave properties throughout the model.

13.4. Initiation of Waves:

We initiate waves (in cells or a network) through simulated stimuli. We can think of stimulus as a input received by our network that triggers an influx of calcium and leads to propagation of calcium waves. This input may be received at a fixed location (in a single compartment) or in a region of a network (multiple cells/ dendrites); it can either be a stationary or a moving input that excites a succession of locations in the network.

We model stimuli in astrocytes with temporal pulses of the G-protein (G_α) which result in generation of InP3 in a region defined in the simulation code. The G-protein concentration during such pulses is represented by G_{in} which appears in equation 11. If stimulus is applied to a point (single compartment) in our model, G-protein pulse is activated for t_{stim} seconds and when it is applied to an area, there is a finite G_{in} value for all compartments within a radius of influence (r_{max}) of the stimulus. Furthermore, the area of stimulus influence can move with velocity Vel_{stim} in time, with pulses applied to successive compartments when they are within the area. All the parameters that define stimulus are given in Table 4, as shown below.

Parameter	Values	Units	Definition
kGI	40	$\mu\text{M} \cdot \text{s}^{-1}$	Rate of InP3 production induced by glutamatergic input
r _{max}	1	μm	Radius of influence
Vel _{stim}	YE/ t _{end}	$\mu\text{m} \cdot \text{s}^{-1}$	Stimulus speed
t _{stim}	1/4 * t _{end}	s	Time of stimulus termination (disappearance)
X _{stim}	-	μm	x-location of stimulus (can be a function of time)
Y _{stim}	-	μm	y-location of stimulus (can be a function of time)
YE	-	μm	Y extent of 2D array (network) of cells
t _{end}	-	s	Total time for simulation

Table 4: Parameters related to stimulus. Changing these parameters we can change the strength or region of influence of stimulus in our network.

14. RESULTS:

In a series of experiments varying different parameters [section 13.2] on different test beds [section 13.1], we examined how each model parameter impacts propagating of Ca waves in dendrites of neurons and astrocytes. In order to better understand the impacts of different parameters on Ca waves, we have divided our analysis into two parts: Qualitative and Quantitative Analysis

14.1. Qualitative Analysis:

Here we analyze qualitatively how does wave behaves on different test beds with change in parameter values. And, these qualitative results are expressed as:

14.1.1. Qualitative Analysis Chart:

We have created a chart of model parameters summarizing effects of parameters on different wave characteristics or factors as mention in previous section.

Parameters	Regeneration	Damping	Wave Speed	Wave Amplitude	Region of Influence
kd1f	Strong Positive	Strong Negative	Strong Positive	Strong Positive	Global
kaa	Positive Indirect	NO EFFECT	Positive	NO EFFECT	Global
fCa	Strong Negative	Strong Positive	Strong Negative	Strong Negative	Global
fInP3	Strong Negative	Strong Positive	Strong Positive	Strong Positive	Global
kCa	Positive	Strong Negative	Strong Positive	Strong Positive	Global
kGI	NO EFFECT	NO EFFECT	Positive	Small Positive	Local
rInP3	Small Positive	NO EFFECT	Small Positive	NO EFFECT	Local
kcbf	Strong Negative	Strong Positive	Strong Negative	Strong Negative	Global
kccb	Strong Positive	Strong Negative	Positive	Strong Positive	Global
Ki2	Strong Negative	Strong Positive	Strong Negative	Strong Negative	Global

Table 5: Chart for model parameters and its effects on the Ca wave dynamics. Strong Positive means that the quantity (like speed) becomes larger or the phenomenon becomes more pronounced when the parameter increase. Strong Negative means that the quantity (like speed) becomes smaller or the phenomenon diminishes as the parameter increase. NO EFFECT means that change in parameter value

have no effect on the wave. Small positive and Small negative means that increase in parameter value will have small (less-strong) impact on the wave. Local and Global means whether the change in parameter value locally will impact locally or globally. All experiments are done on a 100 compartments-long single dendrite, where distance between two compartments is 1 μm and thus length of the dendrite is 100 μm .

Every parameter was varied individually while others were kept constant at their baseline values.

14.1.2. Different Regimes for Calcium waves:

Our experiments demonstrate that there are regenerative, damping and abortive regimes for calcium waves, depending on the physiological parameters. In regenerative regime, calcium waves can travel through the entire network of cells (along dendritic distances) by regenerating itself. In damping regime, calcium waves gets damped as it propagates and could die before it reaches till the end of network. We further observe that abortive regime exist, where our model is not able to generate waves that could propagate even a few micrometers. Table given below gives the different ranges of parameter values that give different wave behavior. Videos for all three regimes can be seen in Appendix B (Figure 13, 14 and 15).

Parameters	Regenerative Regime	Damping Regime	Abortive Regimes	Baseline value
$\text{kd1f (uM.s}^{-1}\text{)}$	≥ 5	$4 < \text{kd1f} < 3$	< 4	5
$\text{Kaa (uM}^2.\text{s}^{-1}\text{)}$	> 4	$4 < \text{kaa} < 2$	< 2	6
$f\text{Ca}$	≤ 0.3	$0.3 < f\text{Ca} < 0.5$	> 0.5	0.3
$r\text{InP3}$	> 0.7	$0.7 < r\text{InP3} > 0.5$	< 0.5	0.7
$k\text{Ca (uM.s}^{-1}\text{)}$	> 500	$500 < k\text{Ca} < 400$	< 400	600
$k\text{cbf (uM}^{-1}.\text{s}^{-1}\text{)}$	< 1	$1 < k\text{cbf} < 4$	> 4	0.7
$k\text{cbb (s}^{-1}\text{)}$	> 5	$5 < k\text{cbb} < 3$	< 3	10
$k\text{i2 (uM}^{-1}\text{)}$	< 1	$1 < k\text{i2} < 5$	> 5	0.0943

Table 6: Table for range of parameter values for different wave behavior. Every parameter is varied separately while keeping other parameters at their baseline value. All experiments were performed on a test bed of two cells with two dendrites (each 10 μm long) each, connect end-to-end. Videos for these regimes can be seen in Appendix B (Figure 13, 14 and 15).

14.1.3. Regenerative Behavior:

We have observed (as shown in Table 5) all the parameters (except $k\text{GI}$) either increase or decrease the strength of regenerative mechanism, while $k\text{GI}$ has no effect.

14.1.4. Damping Behavior:

Among all parameters, kaa , $k\text{GI}$ and $r\text{InP3}$ have no effect on the damping behavior of calcium waves. And, $f\text{Ca}$, $r\text{InP3}$, $k\text{cbf}$ and $k\text{i2}$ increases the damping behavior as we increases their values, whereas kd1f , $k\text{Ca}$, $k\text{cbb}$ decreases the damping behavior.

14.1.5. Wave Speed:

Parameters that increases wave speed are: kd1f , $k\text{GI}$, kaa , $k\text{Ca}$ and $k\text{cbb}$, whereas those decrease it are $k\text{i2}$, $k\text{cbf}$, and $f\text{ca}$.

14.1.6. Wave Amplitude:

We can see from the Table 5 that only two parameters, kaa and $r\text{InP3}$ have no effect on amplitude of calcium waves and all other parameters either increase or decrease wave amplitude.

14.1.7. Region of Influence:

Region of Influence is a qualitative measure to analyze, whether the change in value of given parameter will have impact on waves throughout the model or just locally. We have found that except kGI and rInP3, all parameters have global effect on any change in value, whereas kGI and rInP3 have localized effect. Any change in kGI and rInP3 in a specific region will not affect the dynamics of Ca waves in other regions of model.

This make sense physically as well, because these two parameters (kGI and rInP3) presence is physically limited to the certain region of the model. For example, kGI which defines the strength of stimulus/ input to our model, is active only for t_{stim} sec and that too only in one region (or direction), after which it has zero effect on our model. Similarly, rInP3 which defines the strength of exchange of InP3 between two cells/ dendrites through gap junctions is limited physically as gap junctions are only presents at the interconnections between cells/ dendrites. So, exchange of calcium happens only in certain regions locally.

14.2. Quantitative Analysis of calcium waves in dendrites:

In this section, we show quantitative results for all the experiments, analyzing wave speed and amplitude. Additional material likes videos of wave propagation in astrocyte and neuron dendrite is given in Appendix A.

14.2.1. Astrocytes Model:

In the below given

kd1f	V	fCa	V	fInP3	V	kCa	V	Ki2	V	kcbf	V	kccb	V
8	37.7	1	29.8	1	38.4	1500	105.2	5	20.0	5	0	14	34.4
7	35.7	0.8	30.7	0.8	34.4	1200	95.2	3	24.6	3	15.8	10	33.3
6	33.3	0.6	31.7	0.7	33.3	900	83.3	1	29.8	1	2	6	30.7
4	21.2	0.3	33.3	0.5	28.1	600	33.3	0.5	32.2	0.7	33.3	3	27.0
2	0	0.2	32.7	0.3	19.2	400	-	.09	33.3	0.3	38.4	1	19.4
0	-	0	29.8	0	-	0	-	0	0	0	-	0	19.4

Table 7 and Table 8, we show how wave speed and amplitude change with change in parameter values. The values in first column corresponds to a parameter (for e.g. kd1f) and the values in the next column are speed of waves because of the parameter in first column. Similarly, values in third column corresponds to parameter kaa and values in fourth column are wave speed because of kaa. Wave speed is represented by V ($\mu\text{m.s}^{-1}$) and wave amplitude is represented by A with units in micromolar (μM).

kd1f	V	fCa	V	fInP3	V	kCa	V	Ki2	V	kcbf	V	kccb	V
8	37.7	1	29.8	1	38.4	1500	105.2	5	20.0	5	0	14	34.4
7	35.7	0.8	30.7	0.8	34.4	1200	95.2	3	24.6	3	15.8	10	33.3
6	33.3	0.6	31.7	0.7	33.3	900	83.3	1	29.8	1	2	6	30.7
4	21.2	0.3	33.3	0.5	28.1	600	33.3	0.5	32.2	0.7	33.3	3	27.0
2	0	0.2	32.7	0.3	19.2	400	-	.09	33.3	0.3	38.4	1	19.4
0	-	0	29.8	0	-	0	-	0	0	0	-	0	19.4

Table 7: Table for Wave velocity (V) with change in parameter value. All experiments are done on a 100 compartments-long single dendrite, where distance between two compartments is 1 μm and thus length of the dendrite is 100 μm . Every parameter was varied individually while others were kept constant at their baseline values. Values in red color in every column indicate the baseline value for that parameter. “-“ represents no wave for that set of parameter values. Units for V is $\mu\text{m.s}^{-1}$.

kd1f	A	fCa	A	fInP3	A	kCa	A	Ki2	A	kcbf	A	kccb	A
8	4	1	1	1	3.1	1500	15.4	5	0.9	5	0	14	2.9
7	3.2	0.8	1	0.8	2.6	1200	12.7	3	1.2	3	1	10	2.3
6	2.3	0.6	1.4	0.7	2.3	900	9.7	1	1.8	1	2	6	1.8
4	1	0.3	2.3	0.5	1.8	600	6.1	0.5	2	0.7	2.3	3	1.4
2	0	0.2	3.7	0.3	1.1	400	3.9	0.09	2.3	0.3	3.2	1	0.8
0	-	0	5.8	0	-	0	-	-	2.5	0	-	0	0.7

Table 8: Table for Wave amplitude (A) with change in parameter value. All experiments are done on a 100 compartments-long single dendrite, where distance between two compartments is 1 μm and thus length of the dendrite is 100 μm . Every parameter was varied individually while others were kept constant at their baseline values. Values in red color in every column are the baseline value for that parameter. “-“ represents no wave for those set of parameter value. Units for A is μM .

14.2.2 Neuron Model:

In the below given Table 9 and Table 10, we shows how wave speed and amplitude change with change in different parameter values for neuron model. The values in first column corresponds to a parameter (for e.g. fCa) and the values in the next column are speed of waves because of the parameter in first column. Similarly, values in third column corresponds to parameter rCa and values in fourth column are wave speed because of rCa. Wave speed is represented by V ($\mu\text{m.s}^{-1}$) and wave amplitude is represented by A with units in micromolar (μM).

fCa	V	rCa	V	kcbf	V	kccb	V
1	384.61	100	1.17e+03	5	-	500	400.00
0.8	338.98	50	909.09	3	259.74	200	392.15
0.6	289.85	20	666.66	1	370.37	50	384.61
0.3	196.07	10	512.82	0.7	384.61	10	384.61
0.2	156.25	5	384.61	0.3	400.00	1	377.35
0	-	0	-	0	416.66	0	377.35

Table 9: Table for Wave speed (V) with change in parameter value. All experiments are done on a 100 compartments-long single dendrite, where distance between two compartments is 1 μm and thus length of the dendrite is 100 μm . Every parameter was varied individually while others were kept constant at their baseline values. Values in red color in every column are the baseline value for that parameter. “-“ represents no wave for those set of parameter value. Units for V is $\mu\text{m.s}^{-1}$.

fCa	A	rCa	A	kcbf	A	kccb	A
1	384.61	100	1.17e+03	5	-	500	400.00

1	3	100	5.2	5	-	500	3.2
0.8	3	50	4.8	3	1.8	200	3.2
0.6	3	20	4.2	1	2.8	50	3
0.3	3	10	3.8	0.7	3	10	3.1
0.2	3	5	3	0.3	3.5	1	3
0	-	0	-	0	3.6	0	2.9

Table 10: Table for Wave amplitude (A) with change in parameter value. All experiments are done on a 100 compartments-long single dendrite, where distance between two compartments is 1 μm and thus length of the dendrite is 100 μm . Every parameter was varied individually while others were kept constant at their baseline values. Values in red color in every column are the baseline value for that parameter. “-“ represents no wave for those set of parameter value. Units for A is μM .

14.2.3. Combination of parameters:

In this section, we varied different combinations of parameters together to study how they affected wave speed in a single dendrite. We varied all parameters varied in pairs of two while others were kept at their baseline value as mentioned in

kd1f	V	fCa	V	fInP3	V	kCa	V	Ki2	V	kcbf	V	kcbb	V
8	37.7	1	29.8	1	38.4	1500	105.2	5	20.0	5	0	14	34.4
7	35.7	0.8	30.7	0.8	34.4	1200	95.2	3	24.6	3	15.8	10	33.3
6	33.3	0.6	31.7	0.7	33.3	900	83.3	1	29.8	1	2	6	30.7
4	21.2	0.3	33.3	0.5	28.1	600	33.3	0.5	32.2	0.7	33.3	3	27.0
2	0	0.2	32.7	0.3	19.2	400	-	.09	33.3	0.3	38.4	1	19.4
0	-	0	29.8	0	-	0	-	0	0	0	-	0	19.4

Table 7. All experiments were done on a single dendrite of 100 μm long. Units for wave amplitude is μm and wave speed is $\mu\text{m.s}^{-1}$.

Pair 1: fCa and fInP3			
fCa	fInP3	Wave Speed ($\mu\text{m.s}^{-1}$)	Wave Amp. (μM)
0.5	0.5	15.74	0.6
0.5	1	36.36	1.8
1	0.5	-	-
1	1	31.74	0.8
Pair 2: fCa and kCa			
fCa	kCa	Wave Speed ($\mu\text{m.s}^{-1}$)	Wave Amp. (μM)
0.5	300	-	-
0.5	600	25.97	1
1	300	-	-
1	600	17.85	0.5
Pair 3: fCa and kaa			
fCa	kaa	Wave Speed ($\mu\text{m.s}^{-1}$)	Wave Amp. (μM)
0.5	3	24.09	1
0.5	8	27.77	1.2
1	3	-	-

1	8	21.50	0.5
Pair 4: fCa and kd1f			
fCa	kd1f	Wave Speed ($\mu\text{m.s}^{-1}$)	Wave Amp. (μM)
0.5	3	-	-
0.5	6	33.33	1.7
1	3	-	-
1	6	29.41	1
Pair 5: fInP3 and kCa			
fInP3	kCa	Wave Speed ($\mu\text{m.s}^{-1}$)	Wave Amp. (μM)
0.5	300	-	-
0.5	600	21.27	1.2
1	300	-	-
1	600	38.46	2.4
Pair 6: fInP3 and kaa			
fInP3	kaa	Wave Speed ($\mu\text{m.s}^{-1}$)	Wave Amp. (μM)
0.5	3	20.00	1
0.5	8	22.72	1.2
1	3	37.73	2.4
1	8	39.21	2.6
Pair 7: fInP3 and kd1f			
fInP3	kd1f	Wave Speed ($\mu\text{m.s}^{-1}$)	Wave Amp. (μM)
0.5	3	-	-
0.5	6	27.39	1.8
1	3	-	0.8
1	6	42.55	3.8
Pair 8: kCa and kaa			
kCa	kaa	Wave Speed ($\mu\text{m.s}^{-1}$)	Wave Amp. (μM)
300	3	-	-
300	6	-	-
600	3	33.89	2.36
600	6	34.48	2.5
Pair 9: kCa and kd1f			
kCa	kd1f	Wave Speed ($\mu\text{m.s}^{-1}$)	Wave Amp. (μM)
300	3	-	-
300	6	-	-
600	3	-	-
600	6	34.48	2.4
Pair 10: kaa and kd1f			
kaa	kd1f	Wave Speed ($\mu\text{m.s}^{-1}$)	Wave Amp. (μM)
3	3	-	-
3	6	33.89	2.4
8	3	-	-
8	6	35.08	2.6

14.3. Calcium Wave behavior in Network of Astrocytes:

In following section, we show theoretical and empirical results for wavefront speed in a densely inter-connected network of astrocytes. Refer Appendix C for videos on wave propagation in a 2D network of astrocytes.

14.3.1. Wavefront in a network:

The (random) arrangement of cells (astrocytes and neurons) in our model creates a complicated network/ structure as shown in Figure 9, so that wave propagation is a correspondingly more complicated phenomenon than in a 1-dimensional dendrite. Any such propagation will have rich spatial structure and significantly reduced wave speed. In this section, we review how wavefront (speed is reduced as) wave propagates through a network of astrocytes.

Defining a “wavefront” in a cellular network is an ambiguous task, since there may be moving maxima of calcium concentration in multiple dendrites of a cell when it becomes active. In addition, relative to the case of a wave in a 1-D dendrite, there will be delays due to passage through the cell body and gap junctions, and there will also be mis-alignment between individual dendrites and the overall direction of propagation. To make a simplified computation accounting for the latter, we consider 1) waves as they are passing through dendrites in a network – i.e., the effects of cell bodies and gap junctions are ignored, and 2) make a “plane wave” approximation, which is an approximation to a wavefront with a large radius. It is therefore a crude estimate that is taking into account only the fact that dendrites can mis-align with the overall wavefront direction.

14.3.2. Theoretical computation of wavefront speed:

The approximation of a plane wave (which is actually a linear wavefront in a 2-D network) in a purely dendritic network can be developed as follows.

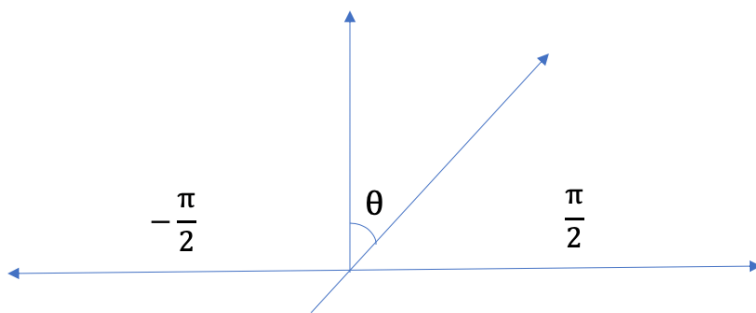


Figure 11: Plane wave approximation. θ is the angle between direction of wave propagation in an individual dendrite and the perpendicular to plane wave. Dendrites are uniformly distributed with respect to θ and can be anywhere from -90° to 90° .

Because of the random orientations, dendrites in our models are distributed uniformly according to the angle they make with respect to the wavefront. We can represent this as a probability distribution $f(\theta)$, with our angular domain going from $-\frac{\pi}{2}$ to $\frac{\pi}{2}$.

$$\int_{-\frac{\pi}{2}}^{\frac{\pi}{2}} f(\theta) d\theta = 1$$

Since, $f(\theta)$ follows uniform distribution, probability density can be represented as constant c .

$$\int_{-\frac{\pi}{2}}^{\frac{\pi}{2}} c * d\theta = 1$$

$$c * \pi = 1$$

$$c = \frac{1}{\pi}$$

We integrate the velocity component perpendicular to the wavefront, $v_{den} \cos(\theta)$, against the uniform distribution.

$$\begin{aligned} v_{avg} &= c * \int_{-\pi/2}^{-\pi/2} v_{den} \cos(\theta) d\theta \\ v_{avg} &= c * v_{den} * \int_{-\pi/2}^{-\pi/2} \cos(\theta) d\theta \\ v_{avg} &= c * v_{den} * \left[\sin\left(\frac{\pi}{2}\right) - \sin\left(-\frac{\pi}{2}\right) \right] \\ v_{avg} &= c * v_{den} * 2 \\ v_{avg} &= \frac{2 * v_{den}}{\pi} \end{aligned}$$

So, this gives us an average dendritic wave speed in a network, where v_{den} is wave speed in a single dendrite. With this estimate, we can say average wave front speed in a network should be approximately equal to 2/3 of the wave speed in a dendrite, ignoring transmission through cell bodies and gap junctions.

Now using wave speed values in a dendrite from Table 8 and Table 10, we can estimate what would be average wavefront speed in a dendritic astrocyte or neural network respectively. For astrocytes, wave speed in a single dendrite with baseline parameter values, represented as v_{den} is $33.33 \text{ } \mu\text{m.s}^{-1}$. So, wavefront speed can be computed as:

$$v_{astrocyte} = \frac{2 * 33.33}{\pi} \cong 21 \frac{\mu\text{m}}{\text{s}}$$

For neurons, wave speed in a single dendrite with baseline parameter values, represented as v_{den} is 416.16 um/s². So, wavefront speed can be computed as:

$$v_{neuron} = \frac{2 * 384.61}{\pi} \cong 256 \frac{\mu m}{s}$$

This gives us a theoretical estimate that is an upper bound for wavefront speed in astrocyte ($v_{astrocyte}$) and neural (v_{neuron}) networks.

14.3.3. Observed Wavefront speed:

In order to compute wavefront speed in a network, we define a wavefront in terms of the (single) most distant compartment in each cell that experiences a calcium wave peak, as follows. As a wave propagates through the cells and spreads across the network, we note the time of activation of the compartment in each cell that is farthest from the origin., i.e., from the point of initiation of the wave. We initiate a wave in the cell body of the centermost cell in our networks (e.g., the cell in row 7 and column 8 in a 13 by 15 network) in all our experiments. Then, distance of that compartment from the origin is divided by time taken for wave peak to occur in that compartment, in order to estimate the speed of the wavefront at that location. This speed is than averaged for all cells in our network, which gives us a mean wavefront speed.

Below are the empirical results from our wave front speed measurement experiments. All the parameters were set to their baseline values as mentioned in Table 6. We can see our empirical results are less than our theoretical results (as shown in section 14.3.2.) and this is because of the delays caused by cell bodies and gap junction transmission.

Network Size (m by n)	Wavefront Speed ($\mu m.s^{-1}$)
3 by 3	16.66
5 by 5	17.34
7 by 7	14.94
9 by 9	14.78
11 by 13	14.67
13 by 15	14.12

Table 11: Table for wavefront speed measurement in different networks of cells (astrocytes). Network of size m by n , have $m * n$ cells, arranged on a grid of m by n . All the parameters were set to their baseline values as mentioned in

kdlf	V	fCa	V	fInP3	V	kCa	V	Ki2	V	kcbf	V	kccb	V
8	37.7	1	29.8	1	38.4	1500	105.2	5	20.0	5	0	14	34.4
7	35.7	0.8	30.7	0.8	34.4	1200	95.2	3	24.6	3	15.8	10	33.3
6	33.3	0.6	31.7	0.7	33.3	900	83.3	1	29.8	1	2	6	30.7
4	21.2	0.3	33.3	0.5	28.1	600	33.3	0.5	32.2	0.7	33.3	3	27.0
2	0	0.2	32.7	0.3	19.2	400	-	.09	33.3	0.3	38.4	1	19.4
0	-	0	29.8	0	-	0	-	0	0	0	-	0	19.4

Table 7 above.

From Table 11, we can say as the network size gets bigger, measured wave front speed decreases and seems to be asymptoting at around $\sim 14 \text{ } \mu\text{m.s}^{-1}$ for large networks.

15. CONCLUSION:

We have studied, modeled and examined calcium wave propagation primarily in astrocytes in three different ways: 1) in individual dendrites, 2) in two interconnected cells with two dendrites each and 3) in a network of up to few hundred cells.

With the parameters values reported in Table 1, we have observed propagation speed in an individual dendrite is in the range $20\text{-}40 \text{ } \mu\text{m.s}^{-1}$, however there are cases where we have observed speed of more than $100 \text{ } \mu\text{m.s}^{-1}$ (shown in

kdlf	<i>V</i>	fCa	<i>V</i>	fInP3	<i>V</i>	kCa	<i>V</i>	Ki2	<i>V</i>	kcbf	<i>V</i>	kccb	<i>V</i>
8	37.7	1	29.8	1	38.4	1500	105.2	5	20.0	5	0	14	34.4
7	35.7	0.8	30.7	0.8	34.4	1200	95.2	3	24.6	3	15.8	10	33.3
6	33.3	0.6	31.7	0.7	33.3	900	83.3	1	29.8	1	2	6	30.7
4	21.2	0.3	33.3	0.5	28.1	600	33.3	0.5	32.2	0.7	33.3	3	27.0
2	0	0.2	32.7	0.3	19.2	400	-	.09	33.3	0.3	38.4	1	19.4
0	-	0	29.8	0	-	0	-	0	0	0	-	0	19.4

Table 7). The lower end of the range is consistent with the speed of the some of the faster calcium waves observed in vertebrate astrocytes [9,10], and our results show that higher speeds are attainable with appropriate parameter values. Wave amplitudes in astrocytes are in the range $1.2\text{-}12 \text{ } \mu\text{m}$ which is consistent with most physiological results in vertebrates.

In a network of astrocytes, however, the net speed of a wavefront that spans many cells will be slower than dendritic speed, because of random orientation of dendrites with respect to wave propagation. Also, propagation of wave through gap junctions and cell body will adds delays. We show this both theoretically (in section 14.3.2) and empirically (in section 14.3.3). As per theoretical estimates, wavefront speed in a network with baseline parameter values is $21 \mu\text{m/s}$ and as per empirical observations, wavefront speed is approximately $14 \text{ } \mu\text{m.s}^{-1}$. This difference between theoretical and empirical results is because of delays added by gap junctions and cell body.

The maximum plausible wave speed in astrocyte dendrites and networks is slow. However, we have observed that speed on a scale of $\sim 100 \text{ } \mu\text{m.s}^{-1}$ can be achieved with higher receptor density, which is conceivable for propagation facilitation. But it is likely that these higher receptor densities are unrealistic. So, we conclude astrocytes network is unlikely be the substrate to support propagating facilitation in the primary lobula of dragonflies, but it is conceivable that such networks might serve this function in smaller subregions of the brain, such as the medial lobula. However, dendritic wave speed in neurons mediated by RyRs has been observed to have much faster dynamics. Waves in the range of $150\text{-}500 \text{ } \mu\text{m.s}^{-1}$ have been observed (refer to Table 9). Thus,

our preliminary conclusion is that neuronal calcium waves may indeed be sufficient to support facilitation at the level of primary lobula.

We modeled intercellular transmission of waves with gap junctions mainly because we assumed this would be the fastest mechanism. However, we observed significant delays as wave travel between cells, and takes a long time to get going. This is due to the fact that it is InP3 that moves through the junction (and not calcium) and because the InP3 receptor kinetic model requires calcium to open, the process of wave regeneration in the post-junction cell depends on the very low levels of calcium present in the target cell, and thus wave takes a long time to get going. Therefore, our original assumption that intercellular transmission happens through gap junctions may not be valid.

16. FUTURE RESEARCH:

Beyond the results presented in this MS Thesis, we recommend few directions in which this project could move and some different approaches that will be explored in coming months.

16.1. Modeling Network of Neurons:

Our work on neurons is limited to dendritic propagation only. We do not model network of neurons. We are not clear on how calcium waves would be transmitted from neuron to neuron, although it might be either by synapses or gap junctions. Furthermore, the neural model is complicated by the fact that calcium entry typically causes depolarization as well. The problem is that depolarization travel faster and it normally cause the neuron to output, so we do not understand why would not that be happening in these cells? Why input-output relationship be governed just be calcium waves?

16.2. Mixture of InP3 and RyR receptor channels in Astrocytes and Neurons:

Both astrocytes and neurons are known to have both types of receptors (InP3 and RyR) [30, 31]. In our current work, in a functional sense, we are really considering *InP3 receptor* and *RyR-dominated* propagation of calcium waves in astrocytes and neurons respectively. In future we could consider cells having mixture of both types of receptors.

16.3. Gliotransmitter based wave transmission:

We have observed intercellular transmission of waves through gap junctions introduce significant delays and thus wave takes a long time to get going. Thus, in future research we will explore other intercellular transmission mechanisms that have faster dynamics. One such mechanism would be gliotransmitter based wave transmission. Gliotransmitters are chemicals released from glial cells that facilitate communication between neurons and other glial cells.

REFERENCES:

1. Corbet, P.S. (1999): Dragonflies: Behavior and Ecology of Odonata. Ithaca, NY: Cornell Univ Press.

2. Nordstrom, K., Barnett, P.D., and O'Carroll, D.C. (2009): Insect detection of small moving targets moving in visual clutter. *PLoS Bolo.* 4:e54. DOI: 10.1371/journal.pbio.0040054
3. Wiederman and O'Carroll, D.C. (2013): Selective attention in an insect visual neuron. DOI: 10.1016/j.cub.2012.11.048.
4. Marisa Brini, Tito Call, Denis Ottolini, and Ernesto Carafoli (2014): Neuronal calcium signaling: function and dysfunction
5. Michael J Berridge 1998: Neuronal Calcium Signaling. DOI: 10.1016/s0896-6273(00)80510-3
6. Dunbier, Wiederman, Shoemaker, O'Carroll (2012): Facilitation of dragonfly target-detecting neurons by slow moving features on continuous paths . DOI: 10.3389/fncir.2012.00079
7. J.E. Castillo and R.D. Grone (2003), A Matrix Analysis Approach to Higher-Order Approximations for Divergence and Gradients Satisfying a Global Conservation Law. *SIAM J. Matrix Anal. & Appl.*, 25, 128–142.
8. Shoemaker (2018): Mechanism for Spatiotemporal Visual Feature Detection in Insects. *Progress Report* 2, March 31, 2018. FA9550-16-1-0153
9. Bazargani and Atwell, (2016): Astrocyte calcium signaling: the third wave. *Nat Neurosci.* 2016 Feb;19(2):182-9. DOI: 10.1038/nn.4201.
10. Jaffe and Creton, (1998): Patterns of free calcium in zebrafish embryos. *J Cell Sci.* 1998 Jun; 111 (Pt 12):1613-22.
11. Scemes E, Giaume C. (2006): Astrocyte calcium waves: What they are and What they do. DOI: 10.1002/glia.20374.
12. Wiedermen (2017): A predictive focus of gain modulation encodes target trajectories in insect vision. *eLife* 2017;6:e26478, DOI: 10.7554/eLife.26478
13. Shuttleworth (2009): Arachidonic acid, ARC channels, and Orai proteins: DOI: 10.1016/j.ceca.2009.02.001
14. Minchul Kang, Hans G Othmer (2009): Spatiotemporal Characteristics of Calcium Dynamics in Astrocytes. DOI: 10.1063/1.3206698
15. James Sneyd and Jean-Francois Dufour (2002): A dynamic model of the type-2 inositol triphosphate receptor. DOI: 10.1073/pnas.032281999
16. Markus Breit and Gillian Queisser (2018): What is required for Neuronal Calcium Waves? A Numerical Parameter Study. DOI: 10.1186/s13408-018-0064-x
17. Johnny Corbino and Jose E.Castillo (2020): High-order mimetic finite-difference operators satisfying the extended Gauss divergence theorem. DOI: 10.1016/j.cam.2019.06.042
18. J. Sneyd (2018): In personal communication over email in regard to Gap junctions.
19. Golovina and Blaustein, (2000): Unloading and refilling of two classes of spatially resolved endoplasmic reticulum Ca^{2+} stores in astrocytes. PMID:10816603
20. Berrideg MJ, 1998: Neuronal Calcium Signaling. DOI:10.1016/s0896-6273(00)80510-3
21. TJ Shutterworth, (2009): Arachidonic acid, ARC channels, and Orai proteins. PMCID:PMC2744097
22. Reyes, Verkhratsky, and Parpura (2012): Plasmalemmal $\text{Na}^+/\text{Ca}^{2+}$ Exchanger Modulates Ca^{2+} -Dependent Exocytotic Release of Glutamate from Rat Cortical Astrocytes. DOI: 10.1042/AN20110059
23. C Agulhon et al., (2008): What Is the Role of Astrocyte Calcium in Neurophysiology? DOI: 10.1016/j.neuron.2008.09.004.
24. Codazzi et al., (2001): Control of astrocyte Ca^{2+} oscillations and waves by oscillating translocation and activation of protein kinase C. DOI: 10.1016/S0960-9822(01)00326-8

25. Parri and Crunelli (2003): The role of Ca²⁺ in the generation of spontaneous astrocytic Ca²⁺ oscillations. DOI: 10.1016/s0306-4522(03)00379-8
26. JJ Omoto (2016): Origins of glial cell populations in the insect nervous system. DOI: 10.1016/j.cois.2016.09.003
27. Karin Nordström, Douglas M Bolzon, David C O'Carroll (2011): Spatial Facilitation by a High-Performance Dragonfly Target-Detecting Neuron. DOI: 10.1098/rsbl.2010.1152
28. Karin Nordström, David C O'Carroll (2011): Small object detection neurons in female hoverflies. DOI: 10.1098/rspb.2005.3424
29. Pradeep Singh 2020: Master's Thesis Codebase. GitHub Repository: <https://github.com/pradeepsinng/h/masters-thesis>
30. P B Simpson, L A Holtzclaw, D B Langley, J T Russell (1998): Characterization of Ryanodine Receptors in Oligodendrocytes, Type 2 Astrocytes, and O-2A Progenitors. PMID: 9589392
31. Tao Li (2018): Dynamic Calcium Release From Endoplasmic Reticulum Mediated by Ryanodine Receptor 3 Is Crucial for Oligodendroglial Differentiation. <https://doi.org/10.3389/fnmol.2018.00162>

APPENDICES:

Appendix A: Calcium Wave in a Single Astrocyte & Neuron Dendrite

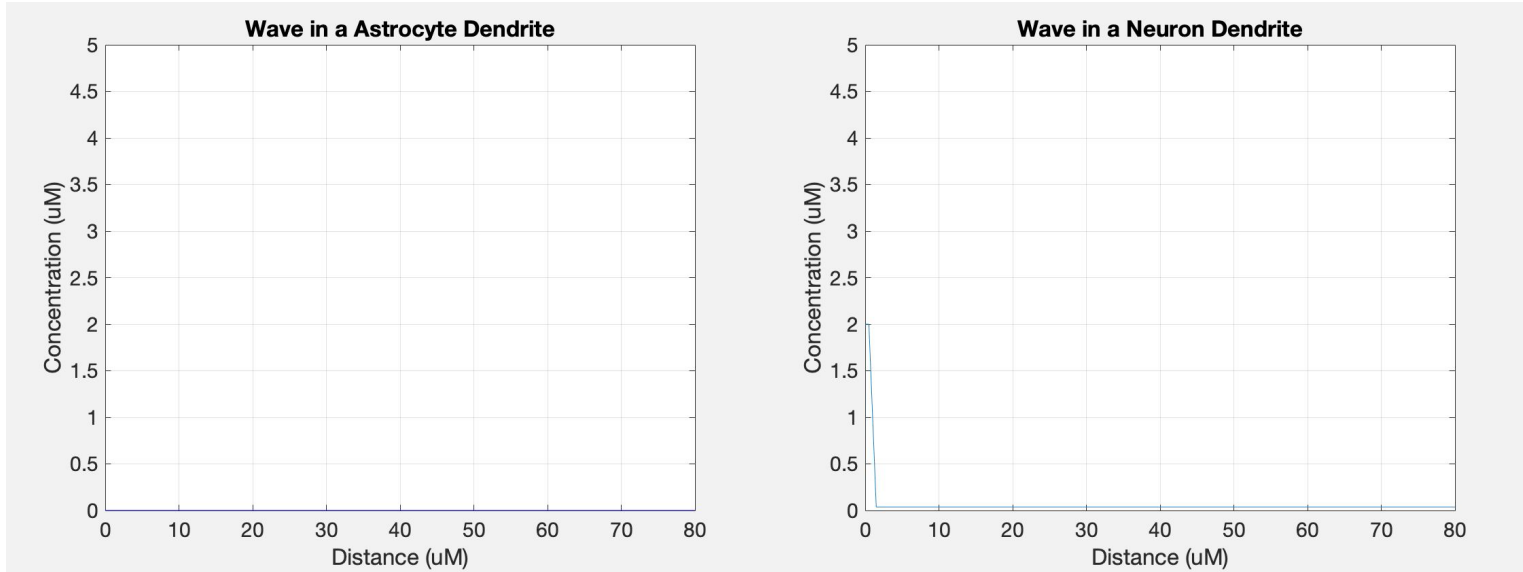


Figure 12: Videos of Ca wave propagation in an single dendrite (80 μm long) of astrocyte and neuron. Wave is initiated on the left end of the dendrite as it gets stimulus and propagates towards the right end. All parameters values for these experiments are set to baseline values (Refer Table 5). To play videos, right click on videos and select play option.

Appendix B: Different Ca wave Regimes

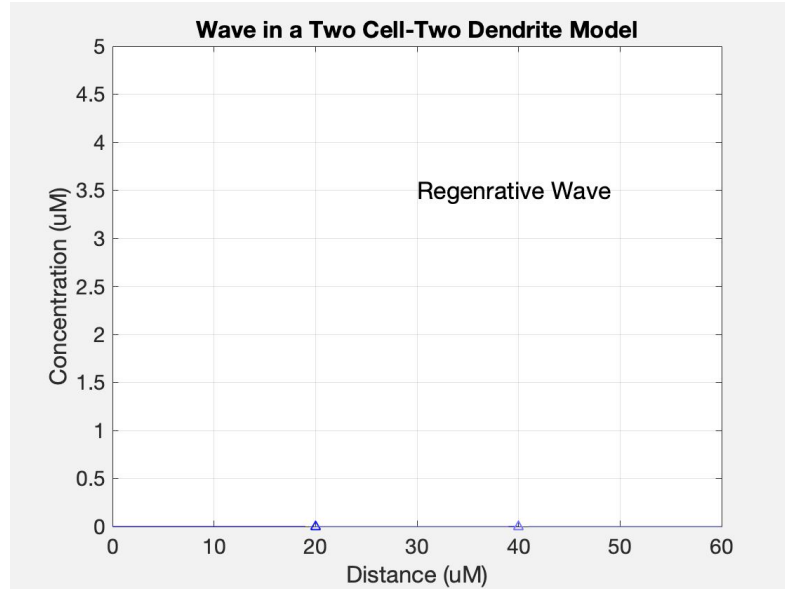


Figure 13: Video of regenerative regime in calcium waves in astrocyte. This experiment is done on a two cell - two dendrite model, where each cell is having two dendrites (one connected on

left and right side) each. Both cells are interconnected through gap junction. Wave is initiated on the left end of the left most dendrite of cell 1. Wave propagates through the cell body of cell 1, right dendrite of cell 1 and then passing to cell 2 through gap junction and eventually reaching the end of cell 2. All parameters values for these experiments are set to baseline values (Refer Table 5). To play videos, right click on videos and select play option.

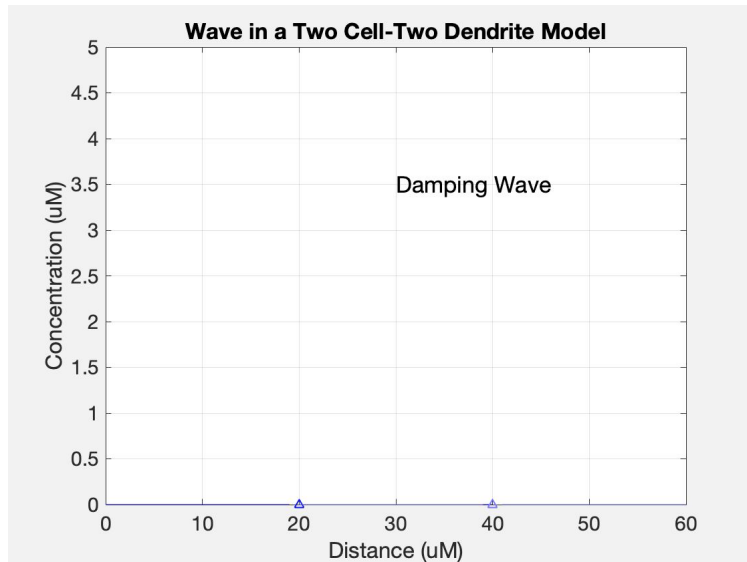


Figure 14: Video of damping regime in calcium waves in astrocyte. This experiment is done on a two cell - two dendrite model, where each cell is having two dendrites (one connected on left and right side) each. Both cells are interconnected through gap junction. Wave is initiated on the left end of the left most dendrite of cell 1. Wave propagates through the cell body of cell 1, right dendrite of cell 1 and then passing to cell 2 through gap junction. In damping regime, wave dies out with some distance, as we can see in this video, wave is not able to cross cell body of cell 2. All parameters values for these experiments are set to baseline values (Refer Table 5). To play videos, right click on videos and select play option.

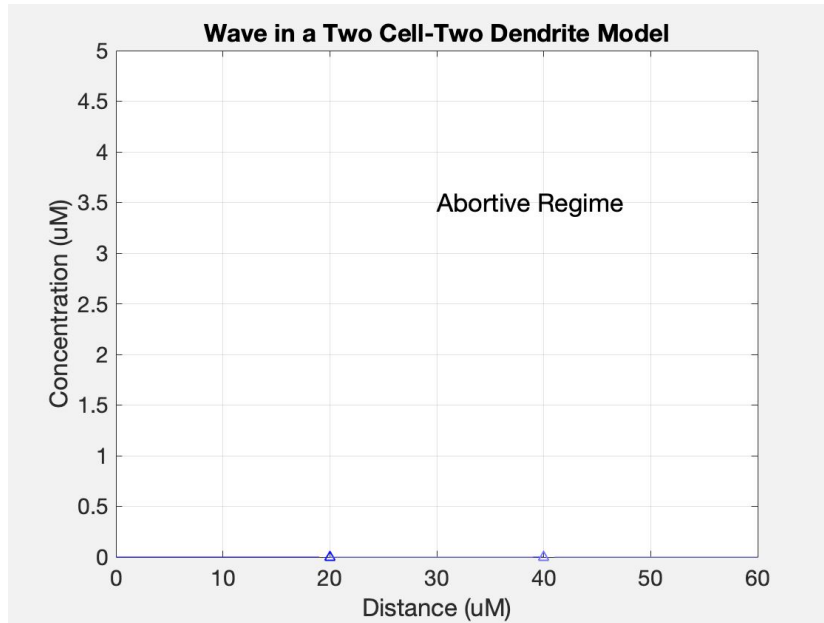


Figure 15: Video of abortive regime in calcium waves in astrocyte. This experiment is done on a two cell - two dendrite model, where each cell is having two dendrites (one connected on left and right side) each. Both cells are interconnected through gap junction. Wave is initiated on the left end of the left most dendrite of cell 1. Wave starts to develop but dies quickly even before it crosses the cell body of cell 1. All parameters values for these experiments are set to baseline values (Refer Table 5). To play videos, right click on videos and select play option.

Appendix C: Astrocyte 2D Network Simulation

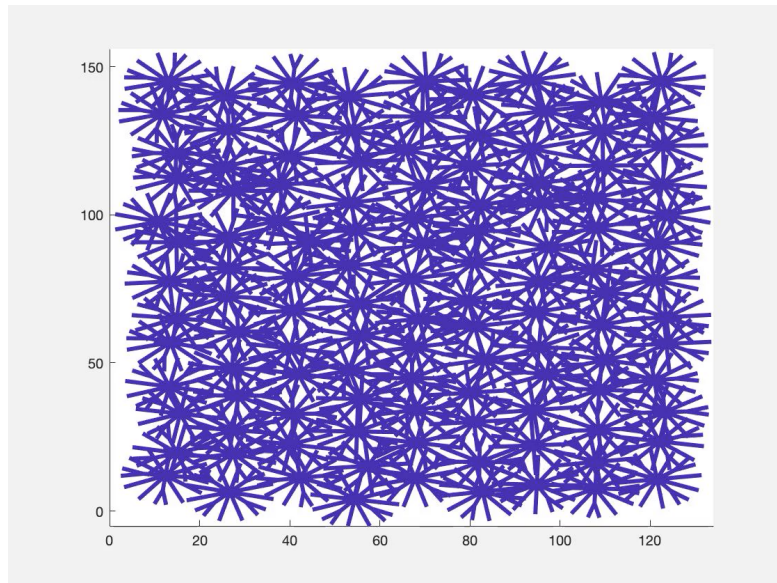


Figure 16: Video for astrocyte 2D network simulation with stimulus moving at a speed 8 um/s. Network of size 9 by 13 cells (in x-y direction), where stimulus acts on X-axis on the 5th cell and moves upward at a speed of 8 um/s. We can see in this simulation that wavefront is circular in shape.

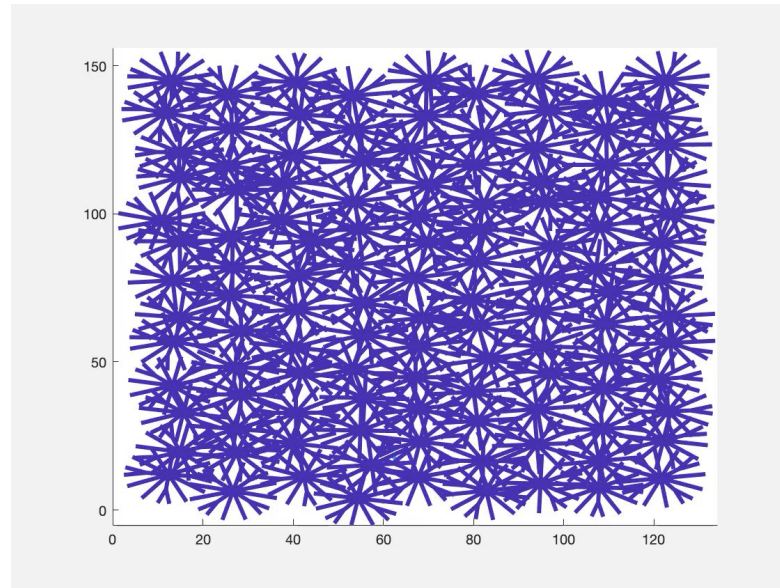


Figure 17: Video for astrocyte 2D network simulation with stimulus moving at a speed 16 um/s. Network of size 9 by 13 cells (in x-y direction), where stimulus acts on X-axis on the 5th cell and moves upward at a speed of 16 um/s. We can see in this simulation that wavefront is somewhat mixture of V-shape and circular shape.

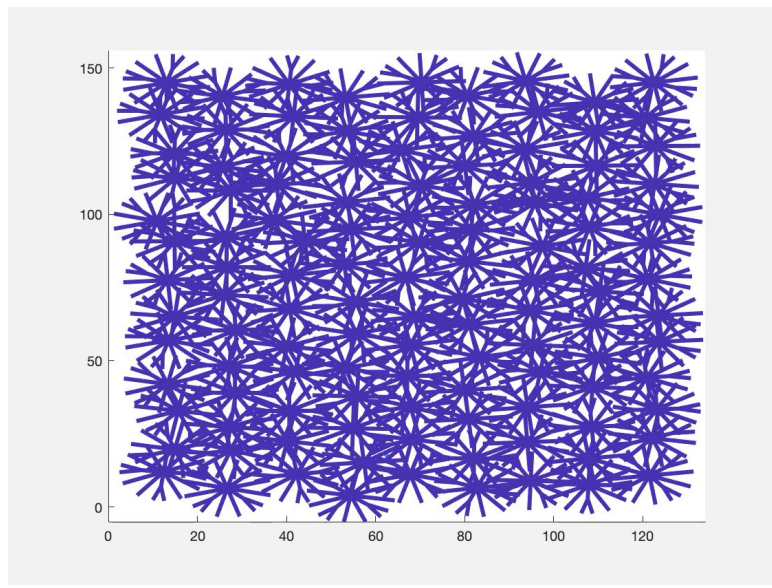


Figure 18: Video for astrocyte 2D network simulation with stimulus moving at a speed 32 um/s. Network of size 9 by 13 cells (in x- y direction), where stimulus acts on X-axis on the 5th cell and moves upward at a speed of 32 um/s. We can see in this simulation that wavefront is in V-shape.